Review

Recent Development on the Study of Supercooled Large Droplets: Impacting, Splashing, Surface Water Dynamics, and Ice Accretion

Yisen Guo , Yang Liu , Mark Sussman , Hui Hu , Yongsheng Lian *

Posted Date: 28 February 2026

doi: 10.20944/preprints202602.2010.v1

Keywords: aircraft icing; drop impact; SLD

 doi:10.20944/preprints202602.2010.v1

Review

Recent Development on the Study of Supercooled Large Droplets: Impacting, Splashing, Surface Water Dynamics, and Ice Accretion

Yisen Guo [1], Yang Liu [2], Mark Sussman [3], Hui Hu [2] and Yongsheng Lian [1,*]

[1] University of Louisville
[2] Iowa State University
[3] Florida State University
* Correspondence: yongsheng.lian@louisville.edu

Abstract

Supercooled large droplets (SLDs), typically defined by diameters exceeding 100 μm, represent a significant meteorological hazard to aviation safety. Unlike conventional cloud-sized droplets, SLDs exhibit higher inertia, causing them to follow ballistic trajectories that result in impingement well aft of standard leading-edge ice protection systems. Furthermore, SLDs are characterized by complex microphysics, including high-speed splashing into secondary droplets and a distinct thermodynamic response where immediate solidification is inhibited, leading to hazardous surface water runback. This paper provides a comprehensive review of recent progress in understanding SLD phenomena. We examine the fundamental mechanisms of droplet impact on dry and wet surfaces, the effects of oblique impingement and ambient air conditions, and the evolution of surface water dynamics. Additionally, the review evaluates the efficacy of emerging ice protection technologies, such as superhydrophobic and liquid-infused surfaces, in mitigating SLD-induced ice accretion. By synthesizing these recent developments, this review aims to bridge the gap between fundamental droplet physics and practical aviation safety strategies.

Keywords: aircraft icing; drop impact; SLD

1. Introduction

Aircraft icing remains a serious weather hazard to aviation safety (Landsberg 2008). Conventional icing scenarios typically involves cloud-sized supercooled droplets with a median volume diameter of 20 μm or less. Although these droplets exist in a meta-stable liquid state below freezing temperatures, their low inertia causes them to follow the aerodynamic streamlines closely. Consequently, their impingement is generally confined to a narrow region near the wing's leading edge. Upon impact, the low thermal mass of these droplets facilitates rapid solidification, resulting in ice accretions that tend to be conformal to the airframe geometry. Because this accumulation occurs primarily within the impingement limits of standard ice protection systems, the resulting aerodynamic degradation is typically manageable for aircraft certified for flight into known icing conditions (Bragg, Gregorek et al. 1986, Poots, Gent et al. 2000, Bragg, Broeren et al. 2005, Landsberg 2008). Furthermore, the physics governing accretion from these small droplets has been extensively characterized, allowing for robust prediction using current numerical and empirical models (Politovich 1989, Bidwell 2005).

1.1. SLD and Its Characteristics

Under meteorological conditions extending beyond standard certification envelopes, aircraft may encounter supercooled large droplets, a regime encompassing freezing drizzle and freezing rain. Defined by diameters exceeding 100 μm, often orders of magnitude larger than typical cloud

 doi:10.20944/preprints202602.2010.v1

droplets, SLDs exhibit distinct aerodynamic behavior governed by their higher inertia. First, unlike smaller cloud droplets, which readily follow the aerodynamic streamlines around the wings, SLDs are less responsive to the pressure gradients. Consequently, they deviate significantly from the local airflow, following more ballistic trajectories that extend the droplet impingement limit well aft of the stagnation region (Politovich 1989). This allows SLDs to strike surfaces beyond the reach of conventional leading-edge ice protection systems (Figure 1), leading to the formation of hazardous, uncontrolled ice accretions (Rutkowski, Wright et al. 2003, Wright and Potapczuk 2004).

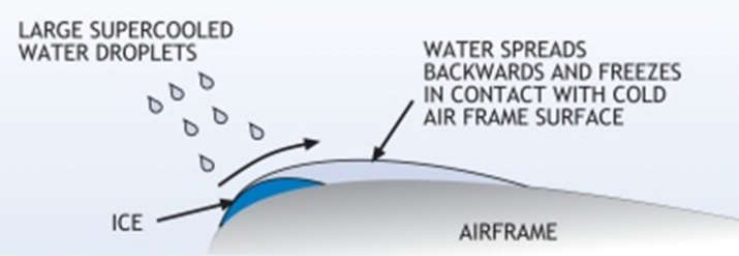

Figure 1. SLD icing on an airfoil surface.

Second, SLDs are also more likely to splash into smaller droplets after impingement (Burzynski, Roisman et al. 2020). The splashed droplets can impinge back onto the wing surface further downstream beyond the regions protected by de-icing devices to cause uncontrolled ice accretion, which can lead to significant decrease in lift and increase in drag. In moderate to severe conditions, an airplane can become so iced up that continued flight becomes impossible (Cebeci and Kafyeke 2003). Droplet splashing is considered as the most important aspect of SLD icing problems, neglecting SLD splashing in previous numerical simulations leads to poor agreement with experimental results (Bond, Potapczuk et al. 2003, Wright and Potapczuk 2004, Anderson and Tsao 2008). While a number of droplet splashing models have been proposed (Rutkowski, Wright et al. 2003, Mani, Mandre et al. 2010, Thoraval, Takehara et al. 2012), most of them only considered normal impact case at relatively low droplet impact speeds. As a result, the proposed splashing models are not applicable for the cases with oblique impacts at high speed that SLDs would experience (Jung and Myong 2013). The characteristics of ambient air, which vary with flight attitude of aircraft and can either suppress or exacerbate droplet splashing, were usually ignored (Xu, Zhang et al. 2005, Xu, Barcos et al. 2007, Latka, Strandburg-Peshkin et al. 2012).

Third, SLDs exhibit a distinct thermodynamic response upon impact compared to typical cloud-sized droplets. Unlike smaller droplets that possess low thermal mass and typically undergo instantaneous solidification upon contact, SLDs retain significant sensible heat and release substantial latent heat during the initial phase transition, thereby inhibiting immediate freezing. Consequently, only a small fraction of the droplet solidifies at the stagnation point. The remaining unfrozen liquid functions as runback water, driven aft by aerodynamic shear forces into regions often exceeding the coverage of leading-edge ice protection systems (Politovich 1989, POTAPCZUK, AL-KHALIL et al. 1993, Bragg 1996). As it convects downstream, this surface water undergoes a complex morphological evolution, initially spreading as a continuous film before coalescing into discrete rivulets, which may ultimately disintegrate into isolated water beads (Anderson and Tsao 2008) (Figure 2). This dynamic mass redistribution renders SLD ice accretion inherently non-linear and computationally challenging to predict.

 doi:10.20944/preprints202602.2010.v1

Figure 2. Experimental study to examine surface water runback over an ice accreting airfoil(Waldman, Liu et al. 2015).

Crucially, the surface water transport governs the local flow velocity and modulates the development of the thermal boundary layer over the accreting surface, thereby dictating the local heat transfer and subsequent freezing rates (Thompson and Marrochello 1999). Unlike conformal ice profiles, this runback phenomenon fosters the growth of hazardous protuberances that penetrate the boundary layer and precipitate severe aerodynamic degradation. Historically, neglecting these runback dynamics in numerical simulations has resulted in significant discrepancies with experimental data (Hansman Jr and Turnock 1989, Wan and Wu 2004, Wright and Potapczuk 2004). Ultimately, the interaction between the boundary layer airflow, unfrozen surface water, ice substrate, and impinging droplets constitutes a highly coupled multiphase system, presenting a challenge for theoretical modeling and simulation.

1.2. SLD Is Aviation Hazard

SLD icing constitutes a critical meteorological hazard to aviation safety, implicated in multiple fatal accidents. Recent climatological assessments indicate that SLD encounters occur with significantly greater frequency than historically estimated (Bragg 1996, Wright and Potapczuk 1996, Wright and Potapczuk 2004). The catastrophic potential of these conditions was tragically underscored by the crash of an ATR-72 in Roselawn, Indiana, on October 31, 1994, resulting in the loss of all 68 lives on board. The subsequent investigation by the National Transportation Safety Board (NTSB) identified the cause as ice forming aft of the de-icing system. The analysis confirmed that this anomalous accumulation was driven not by standard cloud-sized droplets, but by prolonged exposure to SLDs {Bragg, 1996 #190}. Furthermore, SLD icing has been linked to critical instrumentation failures, such as the obstruction of Pitot tubes cited in the 2009 crash of Air France Flight 447, which resulted in 228 fatalities (Vasquez 2009, Stone, Keller et al. 2014).. Consequently, establishing a robust fundamental understanding of SLD phenomenology is a prerequisite for the implementation of effective mitigation strategies. However, despite this urgency, current predictive capabilities for SLD ice accretion remain inadequate (Wright and Potapczuk 2004, Anderson and Tsao 2008, Li, Roisman et al. 2015). This persistent capability gap stems from the drastic disparity between the well-characterized physics of cloud-sized droplets and the complex, inertia-dominated microphysics governing SLD impact and solidification.

1.3. Review Scope

Historically, icing research has predominantly focused on macroscopic observables, such as global ice shapes, impingement limits, and statistical water collection efficiencies. However, the governing micro-physical processes that dictate these outcomes, specifically SLD impact dynamics, rebounding, splashing, surface water runback, and the non-equilibrium freezing process, remain insufficiently characterized (Bond, Potapczuk et al. 2003, Wright and Potapczuk 2004, Anderson and Tsao 2008, Cao, Wu et al. 2014, Zhang, Wei et al. 2015, Liu, Chen et al. 2017, Liu and Hu 2018, Liu, Li et al. 2018, Liu, Ma et al. 2018). To address this fundamental gap, this review provides a comprehensive synthesis of the recent progress in SLD micro-physics. The paper is organized as

 doi:10.20944/preprints202602.2010.v1

follows: Section 2 and Section 3 examine the fundamental mechanisms of droplet impact on dry and wet surfaces, respectively. Section 4 extends this analysis to complex, flight-relevant scenarios, including oblique impingement and multiple-drop interactions. Section 5 evaluates the influence of environmental factors, such as temperature and dynamic surface roughness, while Section 6 reviews the efficacy of emerging ice protection technologies, including superhydrophobic and lubricant-infused surfaces, in mitigating SLD hazards.

2. Drop Normal Impact on Dry Surfaces

2.1. Impact Outcomes

The impingement of a droplet on a flat, dry surface is governed by the competition between inertial, viscous, and capillary forces. Mundo et al. (Mundo, Sommerfeld et al. 1995) experimentally delineated two primary outcomes: lower-inertia drops deposit on the surface to form a coherent liquid film, while higher-inertia drops splash, disintegrating into secondary droplets. They proposed the dimensionless parameter K to define the critical transition boundary between deposition and splashing, formulated as a function of the Ohnesorge (Oh) and Reynolds (Re) numbers:

$$K = (\mathrm{OhRe}^{1.25})$$

$$\mathrm{Re} = \frac{\rho \mathrm{D} \mathrm{V}_0}{\mu}$$

$$\mathrm{Oh} = \frac{\mu}{\rho D (\sigma)^{\frac{1}{2}}}$$

where ρ, μ and σ represent the liquid density, viscosity, and surface tension, respectively, while D and V_0 denote the droplet diameter and impact velocity. From this K-threshold it is easy to tell that inertial forces prompt splash while viscous and capillary forces surpress splashing. Expanding on this binary classification, Rioboo et al. (Rioboo, Tropea et al. 2001) identified six distinct impact regimes, ranging from deposition to complete rebound (Figure 3).

- **Deposition:** Occurs when a drop deforms and stays attached to the surface without breakup.
- **Prompt splash:** Observed mainly on rough surfaces; droplets are generated directly at the contact line during the spreading phase. The droplets are ejected from finger-like jets on the surface. No liftup is necessary.
- **Corona splash:** The spreading liquid is lift up from the surface, and it forms a crown-like lamella. The lamella subsequently breaks up into secondary droplets.
- **Receding breakup:** A wetting phenomenon where some drops are left behind as the liquid retracts from its maximum radius.
- **Rebound and partial rebound:** Occurs when a receding phase is observed, depending on the maximum diameter reached and the receding contact angle.

Their study emphasized that beyond impact kinematics, surface properties such as wettability and roughness play a governing role in determining the outcome. Bartolo et al (Bartolo, Josserand et al. 2006) identified the jetting outcome, where a high-speed vertical jet shoots upwards from the center of the drop upon impact. This occurs on hydrophobic surfaces when the collapsing cavity focuses energy at the center. Tsai, P., et al. (Tsai, Hendrix et al. 2011) shows that on textured surfaces, the outcome isn't just splash or rebound, but can involve localized micro-splashing (fingering) at the pillar scale even if the macro-drop appears to spread.

 doi:10.20944/preprints202602.2010.v1

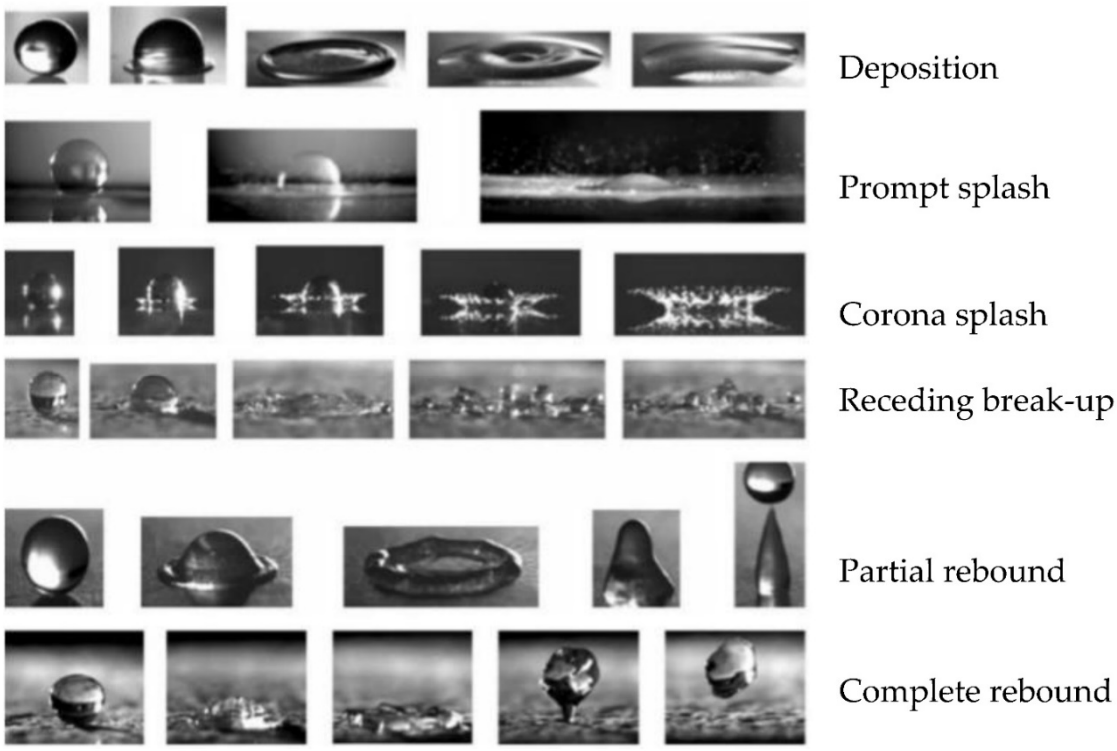

Figure 3. Six distinct outcomes when a drop impacts on a dry surface (Rioboo, Tropea et al. 2001).

2.2. Non-Splashing Regimes: Spreading and Rebound

For non-splashing regimes (spreading, receding, and rebound), analytical models have demonstrated fairly accurate predictive capabilities (Chandra and Avedisian 1991, Xu, Liu et al. 1998, Kim and Chun 2001, Roisman and Tropea 2002). Numerical simulations have also successfully captured experimental behaviors, particularly at lower Weber numbers ($\rho V_0^2 D/\sigma$). Foote (Brant Foote 1973) pioneered the simulation of droplet rebound by solving the Navier-Stokes equations using the Marker-and-Cell (MAC) method. Building on this, Pasandideh-Fard et al. (Pasandideh-Fard, Aziz et al. 2001) utilized the Volume of Fluid (VOF) method to investigate viscous spreading on partially wettable surfaces. They demonstrated that applying a dynamic, variable contact angle boundary condition yielded significantly better predictions of the maximum spreading diameter compared to a constant contact angle assumption. Furthermore, Bussmann et al. (Bussmann, Mostaghimi et al. 1999) successfully extended these numerical approaches to simulate oblique impacts, achieving good agreement with experimental data.

2.3. Splashing Regimes: Thresholds

Early studies shed light on when splashing occurs. Table 1 summarizes various models for drop splash threshold and splashed mass on dry surfaces. Most of the prominent models rely on the Weber number, Ohnesorge number and Reynolds number. These empirical models usually give accurate prediction for normal impacts but not for oblique impacts(Wright and Potapczuk 2004).

Table 1. Drop splash threshold.

	Splash threshold	Range of variables and properties
Mundo et al.(Mundo, Sommerfeld et al. 1995, Mundo, Sommerfeld et al. 1998)	$K = Re^{1/4} \cdot We^{1/2} \geq 57.7$ or $OhRe^{1.25} > 57.7$	Droplet Diameter Range $D_0 = 60 - 150\mu m$ Impact Velocity, $V_0 = 1.3 - 39.3\ m/s$ $K = 133.2 - 186.6$ $We = 620.1 - 1182.0$
Xu et al.(Xu 2007)	$Oh = 3.60Re^{-0.75}$	$D_0 = 3.4 \pm 0.1\ mm$ $V_0 = 3.74 \pm 0.02\ m/s$

 doi:10.20944/preprints202602.2010.v1

Mandre & Brenner(Mandre and Brenner 2012)	$V_0 \geq C\left(\frac{2\sigma^3}{\mu_g^2 \rho D_0}\right)^{\frac{1}{4}}$; $C > 0.3$: $interial\ asymptotic\ regime$ $C < 0.1$: $surface - tension\ dominated$	$\frac{St}{\delta} \approx 0.05 - 0.2$; with $\frac{St}{\delta} = \left(\frac{\rho_l V R}{\mu_g}\right)^{\frac{1}{3}}$
Schmehl et al.(Schmehl, Rosskamp et al. 1999)	$S = \frac{1}{24} Re^{0.162} \cdot We^{0.419} > 1$	
Vander Wal et al.(Wal, Berger et al. 2006)	For dry surface: $\sqrt{Ca} > 0.35$ For wet surface: $\sqrt{We} > 20$ $Oh \times Re^{0.609} > 0.85$: Dry Surface $Oh \times Re^{1.17} > 63$: thin film	$V_0(m/s) = 2.17\sim4.22$ $We = 127\sim1420$ Re = 988 ~ 13900 Ca = 2.91~62.0 $\mu\ (cp)$: 0.409~2.95 $\sigma(dynes/cm)$: 20.1~72.8
Stow and Hadfield(Stow and Hadfield 1981)	$Oh_{splash} = 192Re^{-1.225}$	$1.4mm < D_0 < 4.4mm$ V_0: 2.1~12.41 $m\ s^{-1}$
Palacios et al. (Palacios, Hernández et al. 2013)	$We_c = 26.2Re^{0.433} + 9.96 \times 10^6 Re^{-1.65}$	$1.6 \leq D \leq 3.8\ mm$ $0.5 \leq U \leq 4.75\ m\ s^{-1}$ $786 \leq \rho \leq 1175\ kg\ m^{-3}$ $0.52 \leq \mu \leq 20.42\ mPa\ s$ $20.5 \leq \sigma \leq 70.8\ mN\ m^{-1}$ $100 \leq Re \leq 20{,}000$ $16 \leq We \leq 2000$
Walzel(Walzel 1980) and Schmidt and Knauss(Schmidt and Knauss 1976)	$We \times Oh^{-2.8} > 7.9 \times 10^{10}$ $57.7 = OhRe^{\frac{5}{4}}$	
Hardalupas et al.(Hardalupas, Taylor et al. 1999)	$Oh \times Re^{1.2} > 90$	$160 < D_0 < 230\ \mu m$ $58 < \sigma < 73\ mN/m$ $0.0010 < \mu < 0.0024 \frac{kg}{m\ s}$ $6 < V_0 < 13\ m/s$
Cossali et al.(Cossali, Coghe et al. 1997)	$Oh \times Re^{1.25} > 119.23$	$2 \times 10^2 < We < 1.6 \times 10^3$ $2.2 \times 10^{-3} < Oh < 0.141$ $8 \times 10^{-2} < \delta_{film} < 1.2$
Range and Feuillebois (Range and Feuillebois 1998)	$We > We_{crit} (\approx 310)$, $Oh_{crit} = We_{crit}^{\frac{1}{2}} Re^{-1}$	R_0: $1.94 \pm 0.05\ mm$ $172 \leq We \leq 1111$ $7315 \leq Re \leq 13789$
Vander Wal et al.(Vander Wal, Berger et al. 2006)	$Oh \times Re^{0.609} > 0.85$	D_0: $2.0 \pm 0.06\ mm$ V_0: 2.17 ~ 4.22 m/s μ: 0.409 ~ 3.34 cp σ: 20.1~72.8 $dynes/cm$ ρ: 0.684 ~1.08 g/cm^3
Riboux and Gordillo(Riboux and Gordillo 2014)	$Oh_g We^{\frac{5}{6}}$ for low Oh limit $Oh_g OhRe^{\frac{5}{4}}$ for high Oh limit	V_0: 1.29 ~ 2.28 ms^{-1} $3 \times 10^{-4} \leq \mu \leq 10^{-2} Pa\ s$ $17 \leq \sigma \leq 72\ mN\ m^{-1}$
Roisman et al.(Roisman, Lembach et al. 2015)	$\frac{We}{1+0.24R'^{\left(\frac{1}{2}\right)}} = 29\left(\frac{R_{pk}}{R_{sm}}\right)^{-0.68}$ R_{pk} is the average height and R_{sm} the average width of roughness element, and $R' = \rho R_{pk} U_0 \phi/\mu$	D_0: 1 ~ 3 mm V_0: 0 ~ 8 m/s μ: 1~523 $mPa \cdot s$ σ: 23 ~ 72.75 mN/m ρ: 786 ~1260 kg/m^3
Bird et al.(Bird, Tsai et al. 2009)	$We^{\frac{1}{2}} Re^{\frac{1}{4}} \left(1 - \frac{3.5U_t}{U_n Re^{-\frac{1}{2}}}\right) > 127.0$, U_t and U_n are tangential and normal velocities	D_0: 1.76 ~ 3.4 mm U_n: 1 ~ 4 m/s U_t : − 20~22.5 m/s ν: $1.2 \times 10^{-6} m^2 s^{-1}$ γ: 23 mN/m ρ: 790 kg/m^3
Hao(Hao 2017)	$K \sim \log\left(\frac{R_a}{R_0}\right)$, R_a =arithmetic amplitude average roughness R_0= droplet radius	D_0: 2.3 ~ 3.8 mm V_0: 1 ~ 5.1 m/s μ: 1~1.81 $mPa \cdot s$ σ: 22.9 ~ 72.9 mN/m ρ: 791~998 kg/m^3
de Goede et al.(De Goede, Laan et al. 2017)	$\beta \approx 2.22 \frac{\sqrt{\mu_g}}{\tan(\alpha)} (\rho R)^{\frac{1}{6}} \frac{v_{sp}^{\frac{5}{6}}}{\sigma^{\left(\frac{2}{3}\right)}}$ Or in terms of splashing velocity, $v_s^{\frac{5}{6}} = \frac{\sigma^{\frac{2}{3}} \beta \tan(\alpha)}{2.22\sqrt{\mu_g}(\rho R)^{\frac{1}{6}}}$	V_0: 0.1~4.7 m/s μ: 0.89~2.85 $mPa \cdot s$ σ: 21.8 ~ 72.0 mN/m ρ: 789~997 kg/m^3
Almohammadi and Amirfazli(Almohammadi and Amirfazli 2019)	$Ca - K_2 R^{-\frac{3}{2}} > K_1$ and $Ca < K_3$ $K_1 = 0.06$ $K_2 = 6762$ $K_3 = 1.6$	D_0: 2.5 $\pm$ 0.1 mm V_0: 0.5 − 3.3 m/s μ: 1~100 cSt σ: 20 ~ 70.0 mN/m ρ: 813~1219 kg/m^3

 doi:10.20944/preprints202602.2010.v1

Quetzeri-Santiago et al.(Quetzeri-Santiago, Castrejón-Pita et al. 2019)	$\beta = \frac{\left(1 + \left(\frac{R_{pk}}{R_{sm}}\right)\right)}{1 - \cos(\theta_{max})}$	D_0: 1.9 $\pm$ 0.1 mm (ethanol) D_0: 2.4 $\pm$ 0.1 mm (water) V_0: 1.38 − 2.98 m/s $1790 \leq Re \leq 7152$ $63.48 \leq We \leq 548$
Ashida et al.(Ashida, Watanabe et al. 2020)	$OhRe^{\frac{5}{8}} > K_c$ for corona splash, $K_c = 0.207\left(\frac{\mu_l}{\mu_g}\right)^{\frac{3}{8}}$ $OhRe^{\frac{5}{4}} > K_p$ for prompt splash, $K_p = \left(649 + 3.76\left(\frac{R_a}{D}\right)^{-0.63}\right)^{\frac{5}{8}}$	D_0: 2.16~2.48 mm V_0: 4.2~33 m/s
Burzynski et al.(Burzynski, Roisman et al. 2020)	$Oh < 0.0044,\ We \geq 34Re^{\frac{1}{4}}$	D_0: 2.0~4.0 mm V_0: 6 $\pm$ 26 m/s μ: 0.303~1.24 $mPas$ σ: 22.55 ~ 72.75 mN/m ρ: 790~998 kg/m^3
Zhang et al.(Zhang, Zhang et al. 2021)	$ReOh^{1.3} = 3.8$ for $(Oh < 0.007)$ $(Re - 5.03Re^{0.67})Oh^{1.3}$ for $(Oh > 0.007)$	D_0: 3.7 $\pm$ 0.1 mm D_0: 2.7 $\pm$ 0.1 mm V_0: 1.4 ~ 5 m/s μ: 1 ~ 25.08 $mPas$ σ: 58 ~ 72 mN/m ρ: 0.998 ~ 1.178 g/cm^3
Garci-Geijo et al.(García-Geijo, Quintero et al. 2021)	$We_c \approx \left(\frac{R\cos\theta_0}{\varepsilon}\right)^{\frac{3}{5}}$, ε substrate roughness	$We = 34 \sim 391$

While numerous empirical models exist to predict the splashing threshold, their applicability to aviation icing depends on their behavior in the high-Reynolds-number regime typical of flight. Figure 4 compares the critical Ohnesorge number against the Reynolds number for eleven models. A distinct trend is evident across all models: the Oh_{crit} decreases dramatically as the Re increases up to $Re \approx 2000$. However, beyond $Re \approx 4000$, this rate of decrease slows significantly, and the curves begin to plateau. This transition reveals a shift in the dominant physics governing the splash:

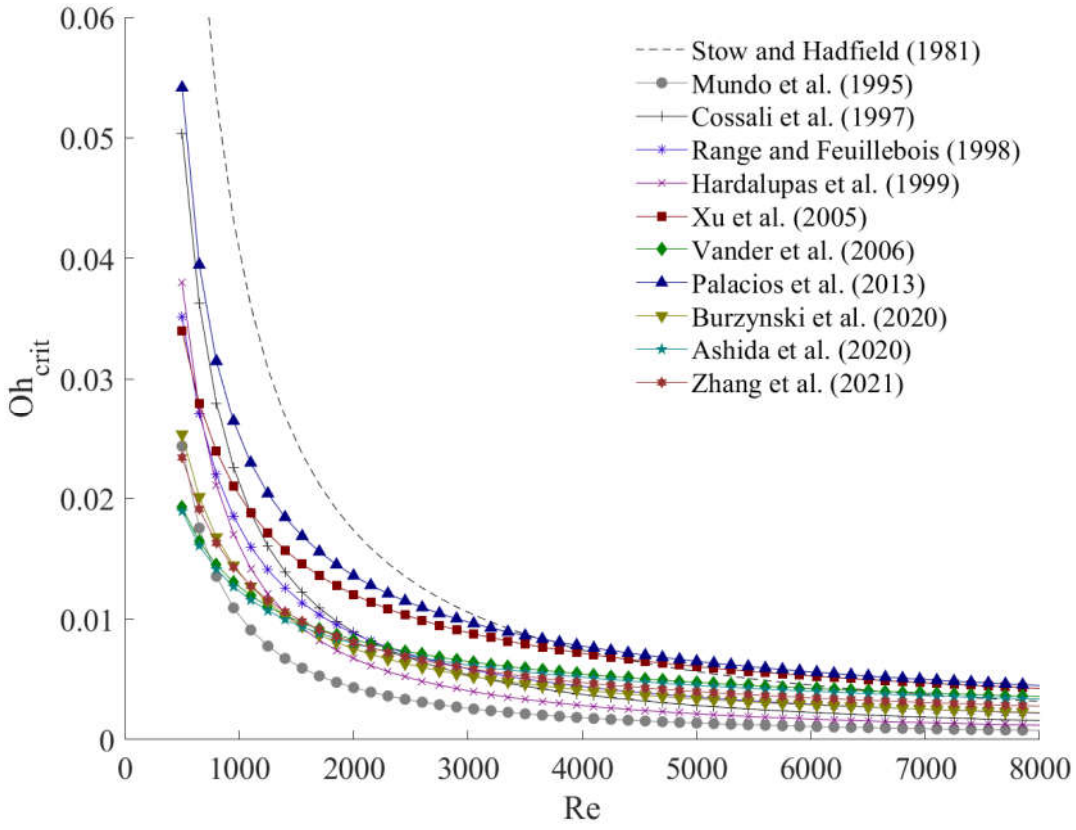

Figure 4. Comparison of different models based on the Ohnesorge (Oh) number vs Reynolds (Re) number correlation.

 doi:10.20944/preprints202602.2010.v1

Low Re Regime ($Re \leq 2000$): The threshold is highly sensitive to the Oh number, which represents the ratio of viscous forces to inertial and surface tension forces. In this regime, material properties, such as viscosity and surface tension, play a critical role in damping the impact energy and preventing splash.

High Re Regime ($Re \geq 4000$): The curves flatten, indicating that the splashing threshold becomes less sensitive to changes in material properties and is instead dominated by the droplet's dynamic behavior (impact velocity and inertia). For SLD icing, which typically involves high-speed impacts corresponding to high Reynolds numbers, the inertial forces overwhelm the viscous dissipation capabilities of the fluid.

For practical SLD simulations, this convergence at high Re suggests that the choice between modern correlations is less critical than for low-speed applications, as most models predict a similar, low asymptotic threshold for splashing. However, older models like Stow and Hadfield (Stow and Hadfield 1981) predict a significantly higher threshold at lower Re, which could lead to under-prediction of splashing mass loss in transitional flow regimes (e.g., near stagnation points or for smaller droplets). Therefore, for robust SLD icing prediction, models that capture this high-inertia asymptotic behavior (such as Mundo et al.(Mundo, Sommerfeld et al. 1995)) are preferable, as they accurately reflect the dominance of dynamic inertial forces over material properties in the aviation environment.

Still, a significant gap remains in the literature regarding high-inertia impacts relevant to aviation and wind turbine icing. While numerous studies have evaluated anti-/de-icing coatings (Séon, Ghabache et al. 2016, Che and Matar 2018, Gordillo, Sun et al. 2018), the majority were conducted at low impact speeds, conditions at least 1 to 2 orders of magnitude lower than those experienced in practical SLD icing events. Among the few who study high drop impact on dry surfaces, Haller et al. (Haller, Poulikakos et al. 2003) developed an analytical model for the high-pressure compression region of high-speed impacts, incorporating a real equation of state to resolve shock propagation. Guo and Lian et al. (Guo, Lian et al. 2016) conducted high-fidelity numerical investigations of droplet impingement at speed greater than 50 m/s, identifying a critical dependency on ambient gas properties. Burzynski et al. (Burzynski, Roisman et al. 2020) experimentally characteritized high-velocity drop impacts on dry surfaces, specifically distinguishing between the prompt splash and the corona splash. They established distinct boundaries for the prompt splash regime and proposed a predictive model for the duration of secondary droplet generation.

2.4. Splashing Mechanism

The fundamental mechanism initiating a splash, particularly in low-speed regions, remains a subject of debate (Jayaratne and Mason 1964, Stow and Hadfield 1981, Fukai, Shiiba et al. 1995, Zhao, Merriman et al. 1998, Bussmann, Mostaghimi et al. 1999, Sussman, Almgren et al. 1999, Weiss and Yarin 1999, Bussmann, Chandra et al. 2000, Zheng and Zhang 2000, Šikalo, Wilhelm et al. 2005, Tanguy and Berlemont 2005). We here list prevelant mechanisms in the literature.

Compressibility & Shock Waves: A prevalent theory attributes splashing to liquid compressibility and the geometric singularity formed by the parabolic interface at the moment of impact (Lesser and Field 1983, Haller, Poulikakos et al. 2003). At very high impact velocities, the liquid cannot be treated as incompressible. A high-pressure shock wave forms upon contact. When this shock wave detaches from the contact line and moves up the droplet free surface, the release of this high pressure drives a high-speed lateral jet (approx 3-5x impact velocity), leading to splash and erosion. However, Mani et al. (Mani, Mandre et al. 2010) argued that this compressible-liquid mechanism is insufficient to explain splashing at lower impact velocities.

Surface Roughness/Asperity Interaction (Prompt Splash): The mechanism for prompt splash involves the immediate ejection of droplets directly from the advancing liquid-solid contact line, rather than from the breakup of a spreading thin sheet. Several papers {Stow, 1981 #50}{Rioboo, 2001 #35} established the causal link between surface roughness and the prompt splash. In these studies,

 doi:10.20944/preprints202602.2010.v1

roughness is typically described as the trigger that causes the advancing liquid sheet (lamella) to break up.

Burzynski et al. (Burzynski, Roisman et al. 2020) demonstrated that the prompt splash is governed by a Rayleigh-Taylor instability of the spreading lamella, making it primarily dependent on liquid properties, in contrast to the corona splash which is driven by aerodynamic effects of the surrounding gas. Latka et al. (Latka, Strandburg-Peshkin et al. 2012) experimentally demonstrated that this specific mechanism is driven by a critical interaction between surface roughness and ambient air pressure. Roughness acts as the primary promoter of the splash, but their study reveals that sufficient air pressure is required to enable the ejection: if the pressure falls below a specific threshold, the prompt splash mechanism is completely suppressed and the drop spreads smoothly. Latka's observation is consistent with Thoroddsen et al. (Thoroddsen, Takehara et al. 2012) who observed prompt splash on smooth dry surfaces, indicating the roughness may not be solely responsible for prompt splash.

Aerodynamic Lift & Air Cushioning (Corona Splash): The corona splash is characterized by the lift-off of a liquid sheet from the substrate, forming a crown that subsequently disintegrates into secondary droplets. The initial lift-off is often attributed to aerodynamic forces (Range and Feuillebois 1998, Riboux and Gordillo 2014) or kinematic discontinuities (Yarin and Weiss 1995).

Other researchers posit that the surrounding gas is the dominant factor. Yarin (Yarin 2006) describes the mechanism as an aerodynamic interaction where the rapidly expanding lamella rides on a trapped cushion of air. As the air rushes out, it exerts an aerodynamic lift force on the leading edge; if this lift overcomes capillary retraction, the sheet levitates and breaks up (Mandre and Brenner 2012). This aerodynamic hypothesis is strongly supported by experimental work from Xu et al. (Xu, Zhang et al. 2005) and Driscoll et al. (Driscoll and Nagel 2011), who demonstrated that lowering the ambient air pressure effectively suppresses splashing. Numerical simulations by Guo et al..(Guo, Lian et al. 2016) further validate the topology of the lifting sheet, though they did not observe the thin intervening air layer postulated by the aerodynamic models.

Mechanism of the Corona Splash: The corona splash is a complex, multi-stage phenomenon driven by significant gas-liquid interaction. Upon impact, the droplet forms a high-velocity liquid lamella that expands radially, displacing the ambient air. This interaction exerts an aerodynamic lift on the leading edge of the sheet. When the ambient gas pressure or density exceeds a critical threshold, the vertical force overcomes surface tension, causing the lamella to elevate from the substrate and form the characteristic crown-like structure. Liu et al. (Liu, Tan et al. 2015) proposed that a Kelvin-Helmholtz instability at the interface between the high-velocity liquid and the stationary ambient air is responsible for the initial destabilization. Their experiments demonstrated that suppressing the air layer effectively stabilizes the interface and prevents splashing.

The subsequent breakup of the elevated corona rim involves a competition between inertial and capillary forces. Agbaglah and Deegan (Agbaglah and Deegan 2014) resolved the debate regarding the governing instability of the rim. Their simulations revealed that while the Rayleigh-Taylor instability (caused by the radial deceleration of the rim) amplifies the growth rate of perturbations, it does not dictate their final spacing. Instead, the wavelength selection and final droplet size remain primarily governed by a Rayleigh-Plateau-like instability, where surface tension acts to minimize the surface area of the fluid rim.

Contact Line Instabilities and Fingering: As the liquid lamella expands radially across the substrate, the contact line frequently exhibits a morphological instability known as fingering. This phenomenon was first theoretically described by Allen (Allen 1975), who attributed the formation of fingers to the Rayleigh-Taylor instability. Allen argued that the deceleration of the rapidly spreading liquid front creates an effective inertial force that drives the dense liquid into the lighter surrounding medium. Although the radial motion is damped by viscous forces, this deceleration is sufficient to destabilize the interface, causing azimuthal perturbations to grow into distinct fingers.

Subsequent experimental studies have validated this deceleration-driven mechanism. Mehdizadeh et al. (Mehdizadeh, Chandra et al. 2004) demonstrated that the wavelength of the

 doi:10.20944/preprints202602.2010.v1

instability aligns with predictions from linear Rayleigh-Taylor theory. Marmanis and Thoroddsen (Thoroddsen and Sakakibara 1998) established scaling laws relating the number of fingers to the Reynolds and Weber numbers, confirming the critical interplay of inertia and viscosity. It is important to distinguish this morphological change from splashing itself: while fingering acts as a precursor, it does not guarantee breakup. However, if the kinetic energy at the finger tips overcomes the capillary retraction force, the fingers will detach to form secondary droplets, transitioning the event into the prompt splash regime (Bhola and Chandra 1999) Recent experimental investigations further demonstrate that this fingering-to-droplet transition can be strongly modulated by interfacial forcing, which alters interfacial stresses and energy redistribution during impact {Ahumada Lazo, 2025 #189}.

2.5. Effect of Ambient Air Pressure

No splashing models in Table 1 take into account the effects of the surrounding air (Bussmann, Chandra et al. 2000). Burzynski and Bansmer (Burzynski and Bansmer 2019) studied different surrounding gases such like Helium (He) and Ammonia (NH_3). For dry surfaces, they found that the most dominant gas property that affects the generation of secondary droplets due to splashing is the density, followed by viscosity of the surrounding gas. They also noted that with the decrease in surrounding gas pressure, the splashing can be suppressed.

Xu et al.(Xu, Zhang et al. 2005) and Latka et al.(Latka, Strandburg-Peshkin et al. 2012) have demonstrated that the ambient air plays a crucial role in determining the splashing behavior of droplets. They discovered that a reduction in air density or pressure can effectively suppress splashing. Xu et al.(Xu, Zhang et al. 2005) showed that reducing ambient pressure can reduce splashing and splash can be completely suppressed in a low pressure environment. Another study also detected that corona splash can be suppressed by making tall pillars on substrate surface even under normal atmospheric condition (Xu 2007), as shown in Figure 5.

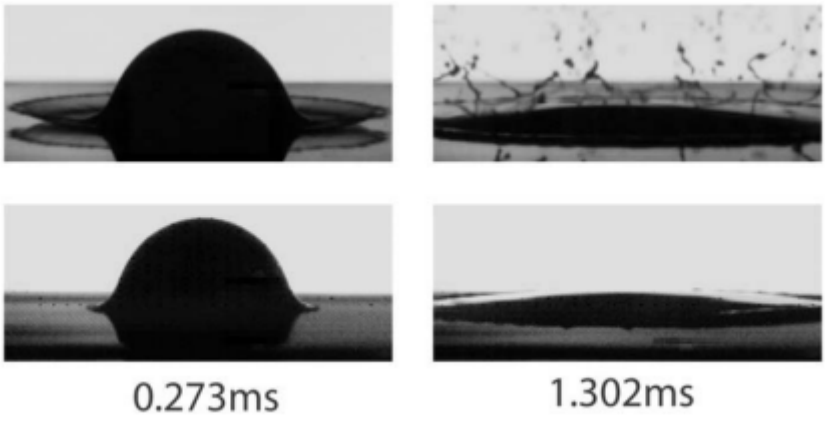

Figure 5. Drop impact at V = 4.3m/s and D = 3.4mm, A corona Splash on Smooth Surface (top) and Splashing is seen to be completely suppressed on a surface consisting of pillars (bottom) (Xu 2007).

Riboux and Gordillo (Riboux and Gordillo 2014) developed a theoretical model to predict droplet splashing while incorporating the effects of ambient air. Numerical simulations by Lian et al.(Lian 2014) (Guo, Lian et al. 2016) investigated the effect of air density on droplet impact. They found that a reduction in air density can lead to attenuation of the splash. Their simulation revealed that a thin film is formed upon contact of the droplet with a solid surface. The thin film moves at a low speed in the vicinity of the solid due to viscous effects, while it moves at a high speed away from the solid. The splashing is caused by the aerodynamic forces acting on the thin film. The thin film splashing is primarily initiated from the pre-existing liquid film on the solid surface, and the liquid content from the droplet sliding along it.

 doi:10.20944/preprints202602.2010.v1

3. Drop Normal Impact on Wet Surfaces

In the context of aviation icing, the dry surface condition is transient; as the aircraft penetrates a cloud, the leading edge rapidly becomes wetted. Therefore, while these dry-surface thresholds are critical for the initial impingement, the wet-surface dynamics discussed in the following sections are more representative of the sustained ice accretion process.

The outcome of a droplet impacting a wetted surface is governed by the interplay of inertial and capillary forces; typically, high-momentum impacts result in splashing, while coalescence or deposition dominates in low-inertia regimes (Rein 1993, Yarin 2006). To characterize the substrate condition, the liquid layer is classified as either a film or a deep pool based on the non-dimensional parameter $\delta = h_0/D_0$, where h_0 is the liquid layer thickness and D_0 is the drop diameter. By convension, the layer is defined as a liquid film when $\delta < 1$ (Cossali, Coghe et al. 1997, Motzkus, Gensdarmes et al. 2009).

Figure 6 illustrates the initial conditions of a drop impacting a pre-existing liquid film of thickness. The post-impact hydrodynamics of a droplet impinging on a thin liquid film are dictated by the physical properties of the liquid phases, specifically density, viscosity, and surface tension, alongside the impact kinematics, including velocity and angle. These governing factors are conventionally consolidated into three dimensionless parameters: the Reynolds number, the Weber number, and the dimensionless film thickness.

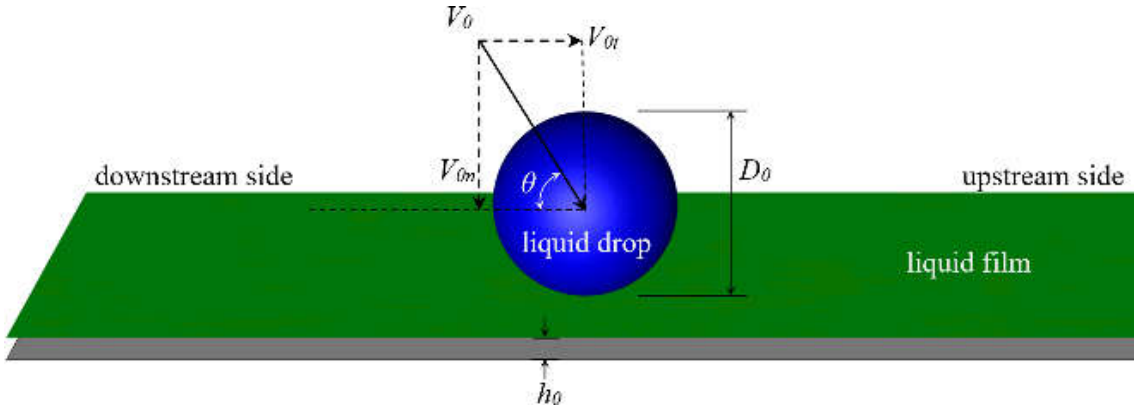

Figure 6. Illustration of drop impact on a thin film(Guo and Lian 2017). V_{0n} is the normal component of the velocity, θ is the impact angle, which dictates the distribution of energy between spreading and lateral jetting.

Experimental investigations (Roisman and Tropea 2002, Josserand and Zaleski 2003, Deegan, Brunet et al. 2007) have classified the resulting motion into distinct regimes. In low-inertia regimes, the droplet deposits onto the liquid film without generating a crown. Conversely, high-inertia impacts induce the formation of a radially expanding crown, the breakup of which leads to splashing. This splashing phenomenon proceeds through a two-stage process (Guo and Lian 2017). The first stage is the ejecta formation in which a horn-shaped jet (ejecta sheet) emerges from the neck region and develops into a rising crown. The second stage is breakup in which instabilities along the crown rim cause the tip to disintegrate, ejecting secondary droplets.

Ribeiro et al {Ribeiro, 2020 #92} identified six distinct outcomes for single-drop impacts on liquid films: deposition, fingering, prompt-splash, crown splash, jetting, and bubble encapsulation (Figure 7).

- Low Energy: The droplet merges with the film via spreading or deposition.
- Moderate Energy: The drop may disintegrate immediately upon contact, resulting in a prompt splash, followed by the ejection of small droplets from the film periphery while the cylindrical crown sheet continues to rise.

 doi:10.20944/preprints202602.2010.v1

- High Energy: Inertia dominates, leading to crown splash, jetting, or rebound. Here, the fragmentation of the crown sheet into small droplets is driven by capillary instabilities (e.g., Rayleigh-Plateau) at the bounding rim (Figure 8)

Early computational efforts to resolve drop impact on liquid films date back to Foote et al. (Brant Foote 1973), who solved the Navier-Stokes equations utilizing the Marker-and-Cell (MAC) method (Brackbill, Kothe et al. 1992). Subsequently, Bussmann et al. (Bussmann, Mostaghimi et al. 1999, Bussmann, Chandra et al. 2000) employed the Volume of Fluid (VOF) method to simulate 3D impacts. Notably, these early models required the introduction of artificial perturbations to trigger splashing, highlighting the challenge of capturing natural instability growth in moderate-resolution simulations.

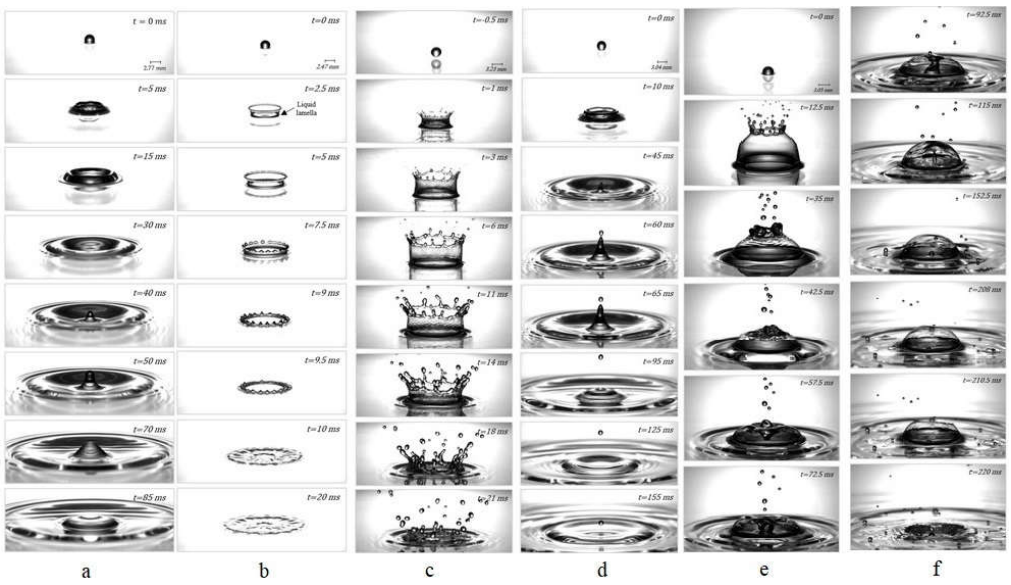

Figure 7. Ribeiro et al(Ribeiro, Silva et al. 2020) has shown the outcomes of drop impacts: a)spreading b) fingering c) crown splash d) jetting e) & f) splashing and bubble encapsulation, respectively.

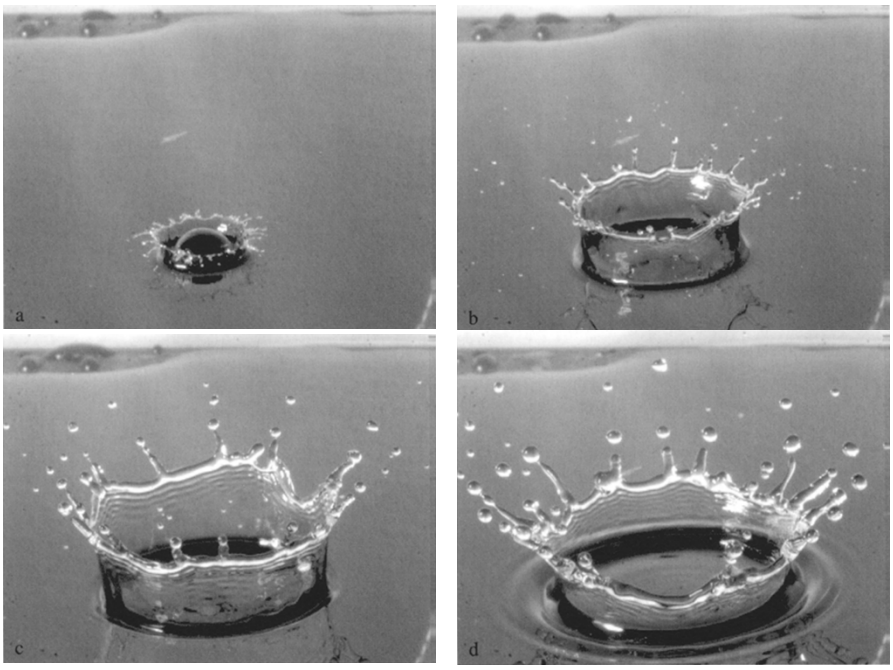

Figure 8. The four stages of splashing a) crown formation and jetting, b) rim instability and jet formation, c) break-up of the jets and formation of secondary droplets, d) crown collapsing period. (Cossali, Coghe et al. 1997).

 doi:10.20944/preprints202602.2010.v1

3.1. Secondary Splashing Morphologies

In a focused investigation of impacts on thin liquid films, Zhu et al. (Zhu, Tu et al. 2021) refined the morphological classification of secondary splashing. By mapping outcomes against the impact parameter K ($K = We/\sqrt{Re}$) and dimensionless film thickness, they identified three distinct variations of the prompt splash regime (Figure 9):

- (a) Active Delayed Splash (PS-ADS): Observed at high impact energies and thinner films, this regime is driven by dominant inertial forces. During the crown's expansion phase, the kinetic energy of the developing fingers exceeds the restraining surface tension. Consequently, the fingers undergo rapid elongation and breakup via the Rayleigh-Plateau instability at the tips while the crown is still spreading radially.
- (b) Passive Delayed Splash (PS-PDS): Occurring at intermediate impact energies, this variation is characterized by a shift from inertial to capillary dominance. While initial fingers form, they lack sufficient momentum to break during expansion. As the crown reaches its maximum diameter and begins to recoil (retraction phase), surface tension pulls the fingers back. The breakup here is triggered by end-pinching.
- (c) Prompt Splash without Delayed Splash (PS-NDS): Found just above the splashing threshold, this outcome represents a state where viscous dissipation prevents droplet separation. Although rim instabilities generate visible fingers, the impact energy is insufficient to overcome surface tension during either the expansion or retraction phases. The fingers eventually retract and merge back into the pool without ejecting secondary delayed droplets.

Their regime map revealed a critical sensitivity to film thickness: increasing the film height was found to suppress the transition to active splashing by enhancing viscous dissipation at the impact crater, thereby requiring significantly higher impact velocities to achieve the same fragmentation outcome.

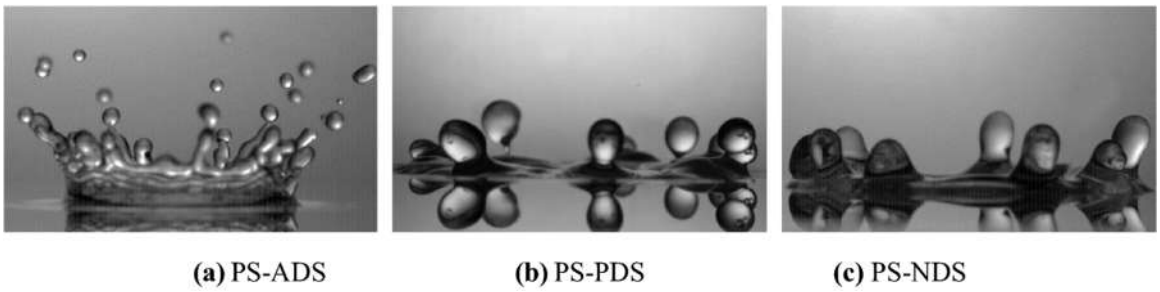

Figure 9. Different splashing phenomena on thin films Prompt Splash-active delay splash (PS-ADS), Prompt Splash-passive delay splash (PS-PDS), Prompt Splash-without delays splash (PS-NDS) (Zhu, Tu et al. 2021).

3.2. Kinematics of the Lamella and Crown Evolution

The impact of a droplet on a liquid film initiates a complex sequence of kinematic events characterized by the formation of a spreading lamella and a bounding rim. Numerical simulations by Rieber et al. (Rieber and Frohn 1999) (We = 250 - 600) revealed a fundamental decoupling between the dynamics of the lamella and its peripheral rim. They established that the basal diameter and shape of the intact lamella are kinematically driven and largely independent of the Weber number.

In contrast, the evolution of the upper rim reflects the balance between inertial stretching and the finite time available for capillary relaxation. At a given temporal instant, higher Weber numbers produce thinner rims and a greater density of secondary structures, including cusps, fingers, and droplets. These findings align with the theoretical frameworks established by Gueyffier et al (Gueyffier and Zaleski 1998) and Yarin et al (Yarin and Weiss 1995)

The propagation of the crown itself is often modeled as a kinematic discontinuity or a jump in velocity and height. Trujillo and Lee (Trujillo and Lee 2001) and Roisman and Tropea (Roisman and Tropea 2002) demonstrated that after an initial transient phase, crown propagation becomes

 doi:10.20944/preprints202602.2010.v1

independent of the upstream droplet flow and is governed primarily by the target film thickness. Through the conservation of momentum, thicker films increase the entrained mass, thereby retarding the radial expansion velocity.

At higher impact energies, the abrupt lateral deflection of the liquid mass generates a high-speed ejecta sheet. Weiss and Yarin (Weiss and Yarin 1999) observed that this jet can either pinch off a toroidal liquid volume at its tip or reconnect with the underlying film surface. This phenomenon was experimentally verified by Thoroddsen et al. (Thoroddsen 2002, Thoroddsen, Thoraval et al. 2011) who noted that the ejecta sheet typically bends downward, rupturing upon contact with the pool surface. This contact triggers a slingshot mechanism, launching droplets in a horizontal trajectory. The secondary atomization mechanisms resulting from these sheets have been extensively characterized, spanning early studies to modern computational analyses (Allen 1975, Fullana and Zaleski 1999, Rieber and Frohn 1999, Roisman, Horvat et al. 2006, Nikolopoulos, Theodorakakos et al. 2007, Krechetnikov and Homsy 2009). (Rao and Basu 2026)

3.3. Parametric Effects on Morphology

In this section, we examine how isolated physical parameters influence droplet impact on wetted surfaces. Subsequently, we evaluate splashing thresholds, which emerge from the synergistic effects of multiple governing variables.

A: Effect of Film Thickness: Vander Wal et al. (Vander Wal, Berger et al. 2006) and Zhu et al. (Zhu, Tu et al. 2021) established that thinner films promote the splashing regime (Figure 10). In these scenarios, the film provides the requisite liquid volume for corona development without offering sufficient depth to effectively dissipate the droplet's kinetic energy. Because the liquid layer is shallow, the impact energy is not absorbed by a bulk volume; instead, it is redirected into high-velocity radial and vertical expansion. This results in:

- **Wider Secondary Sprays:** Droplets are launched further from the impact center due to the lack of vertical momentum absorption.
- **Jet Suppression:** The crown collapse in thin films lacks the necessary inward momentum to form a central jet, as the proximity of the solid substrate restricts the radial inflow required for jet emergence.

As the film thickness increases, the fluid layer begins to act as a momentum sink. Rioboo et al. (Rioboo, Bauthier et al. 2003) noted that beyond a critical thickness, the bulk liquid increasingly absorbs the droplet's kinetic energy through viscous damping and subsurface cavity formation. This leads to a distinct shift in morphology:

- **Splash Inhibition:** The prompt lateral splash is suppressed as the impact energy is partitioned into the displacement of the surrounding bulk liquid.
- **Central Jet Formation:** Unlike thin films, thicker layers provide a sufficient reservoir of fluid. When the impact-induced cavity collapses, the convergence of this larger fluid volume provides the momentum necessary to shoot a prominent central jet upward.

 doi:10.20944/preprints202602.2010.v1

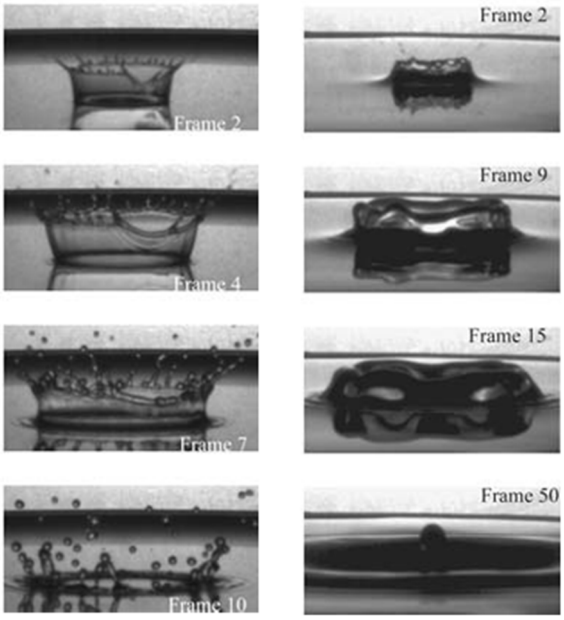

Figure 10. A 2 mm water droplet impacted onto a water film upon an aluminum disk at 3.80 m/s. Left: water film thickness δ =0.1; Right: δ =10.

When the droplet and film consist of different fluids, Chen et al. (Chen, Chen et al. 2017) identified a complex, dual role for film thickness: increasing the thickness of low-viscosity films promotes splashing due to Kelvin–Helmholtz-type instabilities at the interface, whereas increasing the thickness of high-viscosity immiscible films suppresses splashing by acting as an energy-absorbing soft solid

B: Effect of Surface Roughness: Substrate topography plays a critical role in modulating the splashing threshold. Vander Wal et al. (Vander Wal, Berger et al. 2006) demonstrated that surface roughness can fundamentally alter impact dynamics. On smooth substrates, certain impacts may result in stable deposition; however, the same fluid-film system over a rough surface can exhibit both prompt and delayed splashing. This suggests that under these conditions, surface patterning can become the dominant control parameter, superseding both impact energy and intrinsic fluid properties. Zhu et al. (Zhu, Tu et al. 2021) showed that roughness significantly enhances viscous dissipation at the solid-liquid interface. The increased hydrodynamic drag at the substrate curbs the radial expansion of the lamella base. Due to the conservation of mass, this restriction of radial flow forces the liquid to redirect vertically, resulting in a measurable increase in crown height compared to impacts on smooth surfaces.

Morphologically, surface roughness induces a hybrid splashing regime characterized by a non-axisymmetric crown. This structure exhibits circumferential unevenness, with thick, rib-like filaments extending from the base to the rim that provide structural support to the crown film. In this regime, droplet ejection is driven by dual mechanisms: an initial prompt breakup at the filament tips, followed by the Rayleigh-Plateau instability of the elongated filaments as the crown expands. Both mechanisms are driven by the kinematic discontinuities and broken symmetries imposed by the underlying surface texture.

C: Fluid Viscosity and Surface Tension: The outcome of a drop impact is primarily governed by the competition between inertial forces and the stabilizing effects of viscosity and surface tension. Generally, viscosity acts to dissipate kinetic energy and damp the growth of rim instabilities, thereby suppressing the transition to a splash. Similarly, surface tension provides a restorative force that opposes the expansion of the lamella. When the drop and film consist of different liquids, interfacial tension introduces an additional recoiling force, which typically results in smaller crown extensions.

C1: Influence on Crown Dynamics and Splashing

 doi:10.20944/preprints202602.2010.v1

The specific impact of viscosity on crown morphology has been well-documented. Rioboo et al. (Rioboo, Bauthier et al. 2003) established that increasing liquid viscosity significantly raises the energy threshold required for the crown-to-splash transition by damping the instabilities that lead to finger formation on the crown rim. Vander Wal et al. (Vander Wal, Berger et al. 2006) further noted that viscosity and surface tension exert similar influences on the resulting spray, specifically regarding the size and number of secondary droplets. In cases of extreme viscosity, Kittel et al. (Kittel, Roisman et al. 2018) observed that droplets may bypass crown formation entirely, undergoing simple spreading instead. Conversely, low-viscosity wall films have been shown to facilitate rapid crown development and subsequent corona splash.

C2: Effects on Ejecta and Neck Mechanics

Viscosity also dictates the behavior of the liquid during the earliest stages of impact. According to Thoroddsen (Thoroddsen 2002) and Josserand and Zaleski (Josserand and Zaleski 2003), the speed of the intact ejecta sheet decreases as viscosity increases. Josserand and Zaleski (Josserand and Zaleski 2003) highlighted that viscosity is a dominant factor in the neck region, where it dictates the initial width of the ejecta sheet that eventually evolves into the crown wall.

C3: The Interplay of Viscosity and Film Thickness

The relative importance of viscosity changes depending on the impact surface. While viscosity primarily dictates impact outcomes on dry surfaces, it is often superseded by film thickness as the dominant variable when a liquid layer is present (Vander Wal, Berger et al. 2006). However, this dominance is regime-dependent; Wang et al. (2000) discovered that for extremely thin films ($\sigma < 0.1$) the splashing threshold becomes largely insensitive to film thickness, placing the focus back on fluid properties.

C4: Complexities in Multi-Liquid Impacts

When a droplet impacts a film of a different liquid, the interaction is further complicated by viscosity ratios and interfacial tension (Geppert, Chatzianagnostou et al. 2016, Chen, Chen et al. 2017, Geppert, Terzis et al. 2017, Kittel, Roisman et al. 2018). Researh of Bernard et al. (Bernard, Baumgartner et al. 2021) indicates that a high viscosity ratio (droplet is more viscous than the film) can lead to a two-stage crown morphology with the wall-film liquid concentrated at the upper part of the crown. Additionally, viscous losses during the extension phase can dissipate the initial energy, effectively preventing crown extension as much as capillary forces do. Regarding surface forces, a higher interfacial tension ratio acts as a recoiling force that reduces the duration of the ascending phase and results in smaller crown extensions. These interfacial forces also influence the splashing threshold. For instance, miscible liquids may require higher Weber numbers to initiate splashing due to the attenuation of the kinematic discontinuity at the droplet-film boundary.

3.4. The Splashing Threshold

While isolating individual parameters provides a fundamental understanding of fluid behavior, the transition from deposition to splashing is rarely the result of a single variable. Instead, the splashing threshold emerges from a complex interplay between inertial, viscous, and capillary forces. To characterize this boundary, researchers often synthesize these competing effects into dimensionless frameworks. By examining these combined metrics, we can define a critical limit that dictates the stability of the liquid crown across various film depths and fluid pairings.

Several semi-empirical correlations have been developed to predict the transition from deposition to splashing, as summarized in

 doi:10.20944/preprints202602.2010.v1

Table 2 (Yarin and Weiss 1995, Cossali, Coghe et al. 1997, Samenfink, Elsäßer et al. 1999, Deegan, Brunet et al. 2007). However, a comparative analysis reveals significant divergence among these models, even for the fundamental case of water droplets impacting a thin liquid film (Figure 11). Notably, the model proposed by Yarin and Weiss (Yarin and Weiss 1995) predicts a significantly higher threshold velocity for splashing than its counterparts, a discrepancy that becomes particularly pronounced at smaller droplet diameters.

 doi:10.20944/preprints202602.2010.v1

Table 2. Selected splash threshold models for drop impact on liquid film.

	Splash threshold
Yarin and Weiss (Yarin and Weiss 1995)	$V_0^{5/8} D_0^{3/8} \rho^{3/8} \sigma^{-1/4} \mu^{-1/8} > 17$
Cossali et al.(Cossali, Coghe et al. 1997)	$Re^{0.4} We^{0.8} > 2100 + 5880\delta^{1.44}$ for $0.1 < \delta < 1$
Samenfink et al.(Samenfink, Elsäßer et al. 1999)	$Re^{0.162} \cdot We^{0.419} > 24$
Deegan et al. (Deegan, Brunet et al. 2007)	$Re^{0.5} \cdot We > 26000$

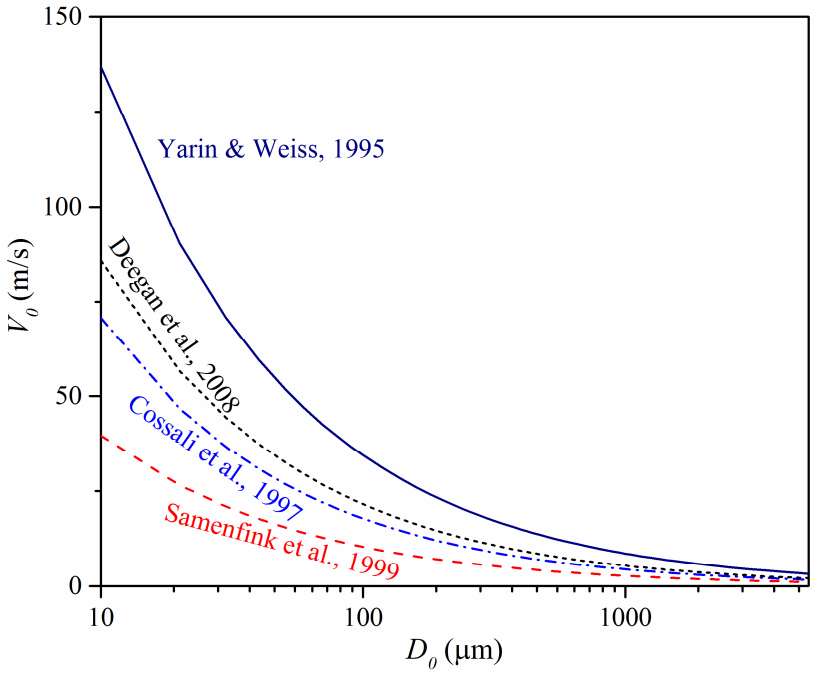

Figure 11. Selected splash threshold models for water drops impact on liquid films of δ = 0.1. The abscissa represents drop diameter and the ordinate represents the corresponding threshold velocity for splash.

Recent research has shifted away from simple curve-fitting toward deriving thresholds based on fundamental physical forces. Riboux and Gordillo (Riboux and Gordillo 2014) proposed a theoretical framework positing that splashing is driven by aerodynamic lift forces acting on the advancing lamella. They formulated a splashing parameter based on the ratio of these lift forces to restraining surface tension, suggesting that breakup occurs once this ratio exceeds a critical constant. While influential, the universality of this model has been questioned; for instance, Goede et al. (De Goede, Laan et al. 2017) demonstrated that this lift-based criterion may not be applicable across diverse fluid types.

The threshold is further modulated by the motion of the target surface. Hao et al. (Hao and Green 2017) examined impacts onto moving substrates and determined that the critical splashing parameter is not static. They observed a reduction in the splashing threshold with increasing tangential velocity, implying that boundary layer shear or the relative motion of the substrate promotes interfacial instability. This finding is of particular relevance to aeronautical applications, as it suggests that splashing occurs more readily on an active wing than under static laboratory conditions.

3.5. Splashing Mechanism on Wet Surfaces

The splashing mechanism on wetted surfaces is not a singular event but rather a hierarchy of fluid instabilities operating across distinct temporal and spatial scales. These transitions move from inertia-driven effects at the moment of impact to capillary-driven breakup during the final stages of atomization.

 doi:10.20944/preprints202602.2010.v1

3.5.1. Stage I: Early-Stage Ejecta and Inertial Instability

At the incipient moments of impact, particularly under high-inertia conditions, the interaction is dominated by a sharp kinematic discontinuity. Vander Wal et al. (Vander Wal, Berger et al. 2006) elucidated that the pre-existing liquid film acts as an inertial barrier, inducing a rapid deceleration of the spreading lamella. This abrupt deceleration of the advancing fluid front generates a strong inertial force equivalent to an effective gravitational field acting across the liquid interface. Because the spreading liquid is effectively pushing against this deceleration into a stationary medium, the interface satisfies the classic criteria for Rayleigh-Taylor instability. Vander Wal et al. argued that this mechanism is primarily responsible for the prompt splash regime, driving initial azimuthal undulations along the nascent crown's rim. These undulations rapidly amplify into finger-like jets that subsequently fragment into fine secondary droplets before a stable corona is fully established.

Krechetnikov and Homsy (Krechetnikov and Homsy 2009) argued that the impulsive, shock-like acceleration favors the Richtmyer-Meshkov instability during these earliest stages, as RT requires more sustained acceleration than a typical impact shock provides.

3.5.2. Stage II: Intermediate Dynamics and Rim Instability

As the flow transitions to the crown formation phase (typically at moderate Weber numbers, We ≈ 200 - 1600), the governing physics shift toward the geometry of the rim. Cossali et al. (Cossali, Coghe et al. 1997) demonstrated that while the bulk expansion of the crown is dictated by the initial kinematic discontinuity, the stability of the toroidal rim itself is capillary-driven.

The rim does not disintegrate spontaneously; instead, it undergoes a Rayleigh-type instability, forming cylindrical jets or fingers protruding from the rim (Rieber and Frohn 1999). Nikolopoulos et al. (Nikolopoulos, Theodorakakos et al. 2005, Nikolopoulos, Theodorakakos et al. 2007) proposed that this is a cooperative process: capillary instability governs the primary formation of these ligaments, followed by surface-tension-driven atomization.

3.5.3. Stage III: Final Atomization

The final stage of the splashing process, i.e., the actual detachment of secondary droplets, is universally governed by the Rayleigh-Plateau (RP) instability. Whether considering the fingers ejecting from a crown rim or the central column in deep-pool impacts, the physics of breakup remains consistent. Castillo-Orozco et al. (Castillo-Orozco, Davanlou et al. 2015) provided experimental confirmation of this mechanism on central jets, showing that surface tension drives the growth of capillary waves along the liquid column. When the amplitude of these waves grows sufficiently to bridge the jet radius, necking occurs, leading to pinch-off and the release of secondary droplets. This RP mechanism serves as the terminal step in the hierarchy, converting the ligaments generated by earlier RT or rim instabilities into the discrete droplets observed in the final splash spray.

This mechanism has been validated by Zhang et al. (Zhang, Brunet et al. 2010), who experimentally measured the spectrum of perturbations on the rim of a crown splash. Their results showed excellent agreement with the theoretical wavelength predicted by the Rayleigh-Plateau mechanism, confirming that the rim breakup is fundamentally a capillary-driven process. Other studies (Fullana and Zaleski 1999, Roisman, Horvat et al. 2006, Nikolopoulos, Theodorakakos et al. 2007) attribute the breakup of ejecta-derived ligaments to this same RP mechanism.

3.5.4. Kinematic Discontinuity and Crown Propagation

Beyond instabilities themselves, the propagation of the crown itself is modeled as a kinematic discontinuity. Trujillo and Lee (Trujillo and Lee 2001), effectively aligning with Yarin and Weiss (Yarin and Weiss 1995), described the crown as a propagating jump in velocity and height. Their analysis (Re = 500 - 5000) demonstrated that after an initial transient phase, crown propagation becomes independent of the upstream drop flow and is governed solely by the target film thickness. Thicker films increase the entrained mass, retarding radial velocity through momentum

 doi:10.20944/preprints202602.2010.v1

conservation. Roisman and Tropea (Roisman and Tropea 2002) later confirmed that in high-velocity impacts, liquid inertia dominates this process, rendering viscous discrepancies between various models (e.g., Trujillo vs. Yarin) negligible.

3.6. Mass Loss and Re-Impingement Hazard

The critical parameter for SLD icing simulations is the mass loss ratio ($R_m = m_s / m_0$, m_s is the splashed droplet mass, m_0 is the impact drop mass), representing the fraction of the incoming droplet mass that is ejected. Unlike dry surface splashing, where mass loss is typically limited (e.g., < 25%), wet surface splashing can result in mass loss ratios exceeding 75%. This ejected mass does not vanish but re-enters the freestream, often re-impinging aft of the protected leading edge.

Figure 12 compares the mass loss from splashing on wet surface as a function of *K* value with existing empirical models. Although the models of Samenfink et al (Samenfink, Elsäßer et al. 1999). and Schmehl et al.(Schmehl, Rosskamp et al. 1999) predict that splashing occurs at the same *K* value, the model of Samenfink et al.(Samenfink, Elsäßer et al. 1999) predicts higher splashed mass than the model of Schmehl et al. (Schmehl, Rosskamp et al. 1999). Figure 12 also indicates that the numerical result of Guo et al. (Guo, Lian et al. 2016) matches well with the prediction of Honsek et al. (Honsek, Habashi et al. 2008), which predicts that splashing occurs at a much larger *K* value.

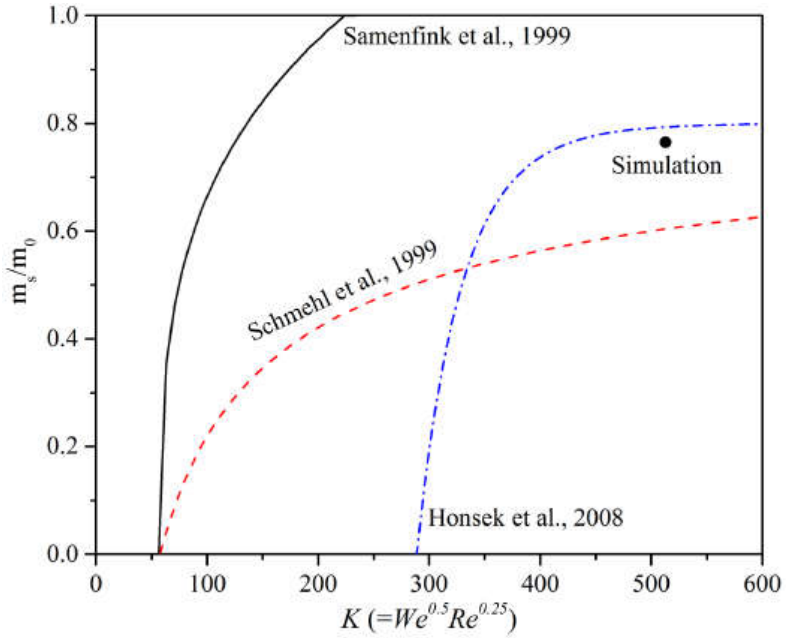

Figure 12. Comparison of mass loss from splashing with empirical models(Guo, Lian et al. 2016).

3.7. Effect of Ambient Air

Shetabivash et al. (Shetabivash, Ommi et al. 2014) numerically demonstrated that increasing ambient gas density retards the evolution of both crown radius and height due to increased aerodynamic drag. However, gas viscosity was found to have a negligible effect on the radial evolution rate.

Guo et al. (Guo, Lian et al. 2016) investigated the effect of surrounding gas on thin film splashing numerically. In their study, the impact of a 50-μm diameter water drop onto a uniform thickness water film with the impact velocity of 78 m/s was simulated and the film thickness was assumed to be 2 μm according to experiments by Zhang and Hu (Zhang and Hu 2014). Thin film splashing is found to be less affected by ambient air than dry surface splashing but has a much larger splashed mass loss. In contrast to the dry surface cases, there is no significant difference in splashing suppression when the ambient air density is reduced. Nonetheless, the tip of the lamella moves

 doi:10.20944/preprints202602.2010.v1

slightly faster outward at lower air density than at higher air density. The lower density air provides less resistance to the expanding lamella.

4. Complex Impact Scenarios

4.1. Oblique Drop Impingement

Most existing literature has focused on normal impact conditions characterized by relatively low impact velocities (< 10 m/s) and dimensionless film thicknesses δ greater than 0.1 (Rein 1993, Yarin and Weiss 1995, Cossali, Coghe et al. 1997, Samenfink, Elsäßer et al. 1999, Weiss and Yarin 1999, Thoroddsen 2002, Rioboo, Bauthier et al. 2003, Cossali, Marengo et al. 2004, Yarin 2006, Mukherjee and Abraham 2007, Nikolopoulos, Theodorakakos et al. 2007, Motzkus, Gensdarmes et al. 2009, Shetabivash, Ommi et al. 2014). In contrast, studies investigating high-speed oblique impact on thin liquid films remain rare.

Impact on Deep Pools (δ > 1): Among the few studies addressing oblique impact, early work by Ching et al. (Ching, Golay et al. 1984), Leneweit et al. (Leneweit, Koehler et al. 2005) and Zhbankova and Kolpakov (Zhbankova and Kolpakov 1999) focused on deep liquid pools in the non-splash regime. Leneweit et al. (Leneweit, Koehler et al. 2005) observed that oblique impingement initially results in coalescence followed by interface depression. They identified a Weber number threshold of 10 governing the transition from convex capillary wave generation to the ejection of a lamella from the impact site. Conversely, Ching et al. (Ching, Golay et al. 1984) found that while droplet streams could bounce, single drops could not. They hypothesized that the disturbances on the liquid surface created by previous drops are necessary for bouncing, whereas a single drop dissipates most of its kinetic energy in crater formation, leaving insufficient energy for rebound.

Studies on Moving and Oblique Surfaces: Several studies have utilized moving substrates to simulate oblique impact dynamics. Cheng and Lou (Cheng and Lou 2015) investigated oblique impact on both stationary and moving walls. As illustrated in Figure 13, the stationary oblique wall experiments produced an asymmetric splash with an elliptical lamella, where crown fingers extended radially outward while spikes on the downstream side exhibited significant curvature. They developed a phase diagram correlating the moving wall speed with splashing phenomena. Similarly, Alghoul et al. (Alghoul, Eastwick et al. 2011) used a moving film setup to create an effective oblique impact angle. They reported an asymmetrical impact structure that became more symmetrical over time, while initially inclined in the direction of film motion. Notably, they observed that the height of the resulting jet increased with film height.

Hao and Green (Hao and Green 2017) further revealed that on a moving substrate, corona splash could be suppressed to a prompt splash. They also noted that reductions in ambient pressure could cause a transition from splashing to deposition. They hypothesized that aerodynamic lift forces acting on the lamella's leading edge are responsible for driving the separation that leads to splashing.

More recently, Bao et al.(Bao, Yi et al. 2025) and Stober et al.(Stober, Santini et al. 2025) experimentally studied oblique droplet impacts on thin wall films. Their findings are similar at the level of physical mechanisms, including asymmetric crowns, front dominated splashing, and the importance of normal inertia and impact angle. Bao et al. provided thin film crown metrics and a K number based splashing threshold, while Stober et al. provided threshold formulas using impact angle and We for comparable oblique thin film impacts.

Numerical approaches have provided additional insights into the internal dynamics of oblique impact. Cheng and Lou (Cheng and Lou 2015) employed a Lattice-Boltzmann model to study impacts at angles between 30° and 90°, observing a transition from crown splashing to single-sided splashing induced by cosine-wave perturbations on the drop surface. Guo and Lian (Guo and Lian 2017) revealed that shallower impact angles lead to a smaller lamella on the downstream side and suppressed lamella development upstream (Figure 14). They attributed this to the origin of the liquid: the downstream lamella is formed primarily from the liquid film. Consequently, a thinner film results in a thinner, and less stable lamella that breaks up earlier. Conversely, on the upstream side,

 doi:10.20944/preprints202602.2010.v1

increasing film thickness creates a thicker lamella with greater inertia. This increased inertia allows the lamella to resist aerodynamic drag more effectively, making the upward motion more prominent.

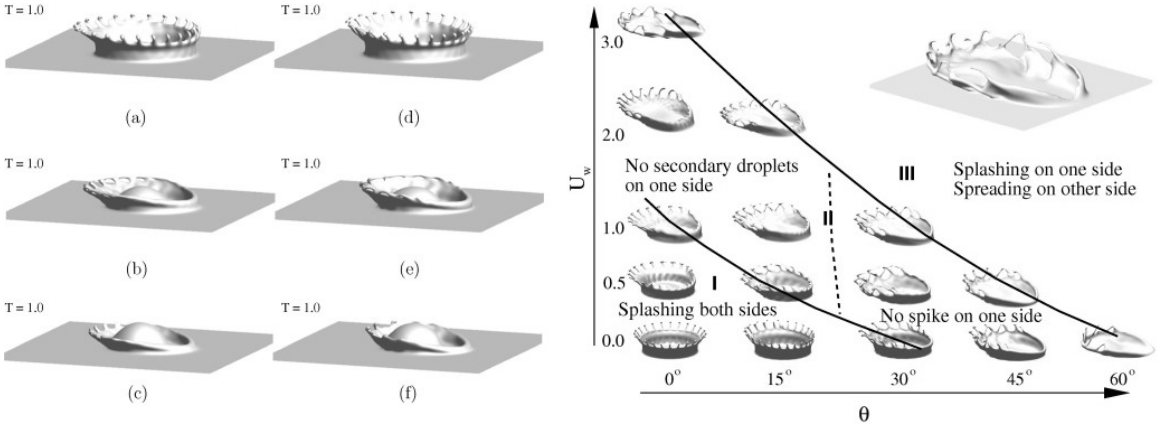

Figure 13. Cheng and Lou(Cheng and Lou 2015) showed the comparison of the shapes of the splashing lamella on a stationary wall and a moving wall at. (a) $\theta = 15°(stationary\ wall)$, (b) $\theta = 45°(stationary\ wall)$, (c) $\theta = 55°(stationary\ wall)$, (d) $\theta = 15°(moving\ wall)$, (e) $\theta = 45°(moving\ wall)$, (f) $\theta = 55°(moving\ wall)$. The right section shows the correlation between speed of moving wall and the impact angle of the drop that results in different types of splashes.

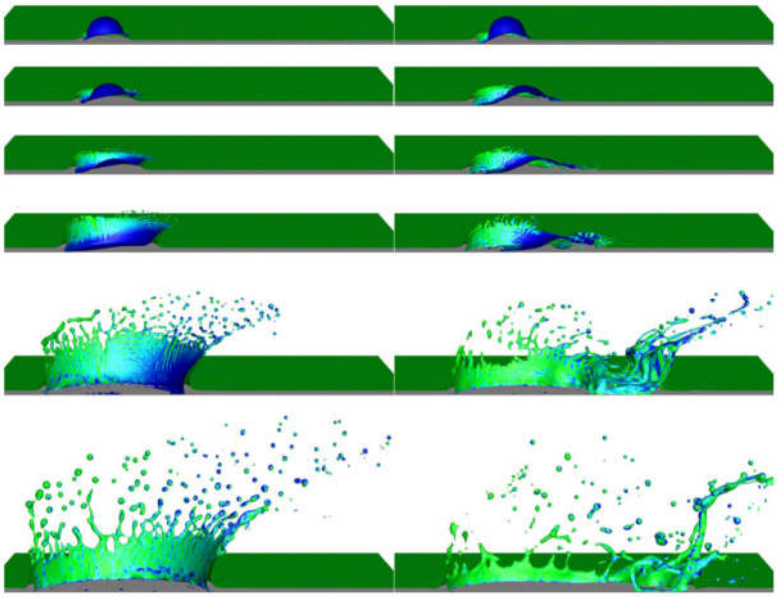

Figure 14. Oblique impact of 41.3-μm-diameter water drop on 5-μm-thick water film. Left: impact angle is 60° ($V_{0_{normal}}$ = 53 m/s and $V_{0_{tangential}}$= 30.6 m/s). Right: impact angle is 30° ($V_{0_{normal}}$ = 53 m/s and $V_{0_{tangential}}$ = 91.8 m/s) (Guo and Lian 2018).

Effect of Impact Angle and Fluid Properties: The influence of impact angle and fluid properties have been quantified in several extensive studies. Okawa et al. (Okawa, Shiraishi et al. 2008) analyzed over 500 cases, revealing that when the angle between the primary drop velocity and the surface normal was less than a critical threshold of 50°, increasing the impingement angle significantly increased the total mass of secondary drops. However, beyond this critical angle, secondary droplet formation ceased. Liang et al. (Liang, Guo et al. 2013) examined the role of surface tension and viscosity on inclined wetted substrates. They observed asymmetrical splashing and noted that increasing surface tension led to larger secondary droplet sizes. Furthermore, they identified a viscosity-dependent transition, where low viscosity fluids exhibited prompt splash while higher viscosity fluids displayed delayed splashing.

 doi:10.20944/preprints202602.2010.v1

Implications for Icing and Efficiency: Since swept wings predominantly experience oblique impacts, relying solely on normal impact correlations (such as those typically cited in literature) is likely to yield inaccurate predictions of water collection efficiency. A robust understanding of these oblique dynamics is therefore essential for accurately predicting runback water extent and subsequent mass loss in practical SLD scenarios.

4.2. Multiple-Drop Impact

Normal Impact: While single-drop studies provide fundamental insights, the practical reality of aircraft icing involves the impact of a continuous flux of droplets. In this regime, droplets rarely impact a quiescent surface. Instead, they impinge upon a dynamic liquid layer generated by previous impacts, leading to complex crown-crown interference phenomena. Roisman et al. (Roisman, Prunet-Foch et al. 2002) characterized these interactions on dry surfaces, identifying droplet spacing as the governing parameter for the resulting film flow.

Extending this to wetted surfaces, Raman et al.(Raman, Jaiman et al. 2015) and Li et al. (Li, Jia et al. 2016) utilized the two-dimensional Lattice Boltzmann method to investigate the normal impingement of droplet pairs. Their simulations revealed that the collision of expanding crowns generates a distinct middle splash or central updraft. Raman et al. (Raman, Jaiman et al. 2015) found that the height of this central ejecta is inversely related to the dimensionless horizontal spacing. As drops impact closer, the constructive interference of the crowns intensifies. Li et al. (Li, Jia et al. 2016) demonstrated that non-simultaneous impacts break the flow symmetry. They noted a complex non-linear relationship between droplet diameter and spacing, where the interaction intensity initially increases and then decreases as the horizontal distance grows, creating a specific window of maximum instability.

Oblique Interactions: In flight conditions, multiple impacts are almost invariably oblique. Guo and Lian (Guo and Lian 2018) simulated high-speed droplet pairs (V_0 = 75 m/s) at impact angles of 30° and 60° to decouple the effects of tangential momentum (Figure 15). The low angle (30°) case is dominated by horizontal shear. No downstream crown forms, and the upstream crown is stunted. The interaction between the two drops is relatively weak as the horizontal momentum convects the fluid downstream before significant crown-crown collision can occur. In the high angle (60°) case the flow topology shifts drastically. The interacting lamellae twist into a complex S-shape, breaking up into elongated ligaments. The lower region of this S-structure moves horizontally downstream, while the upper region is driven upward, leading to a dual-mode breakup that significantly enhances secondary droplet production.

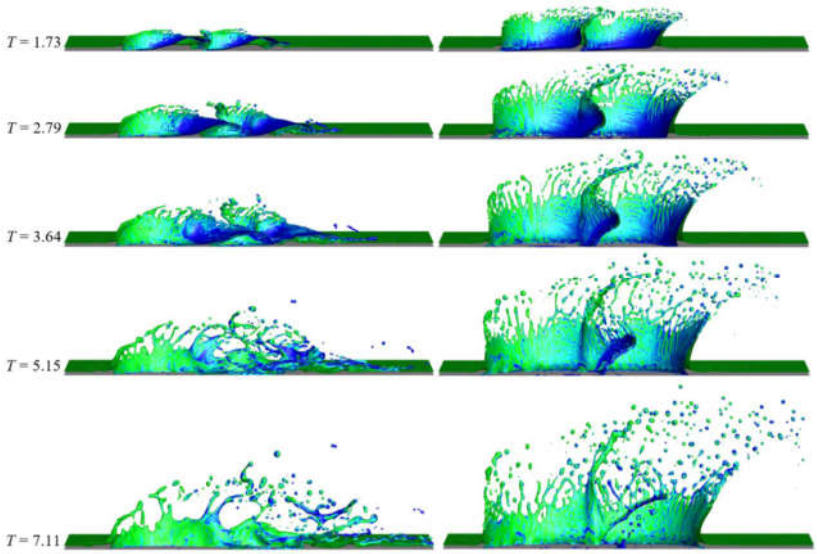

Figure 15. Comparison of high-speed drops impacts with 30° and 60° impact angles (D_0 = 41.3 μm, h_0 = 5 μm, V_0 = 75 m/s). Left: θ = 30°; right: θ = 60°(Guo and Lian 2018).

 doi:10.20944/preprints202602.2010.v1

Simultaneous vs. Successive Mechanisms: Liang et al. (Liang, Guo et al. 2013, Liang, Zhang et al. 2018, Liang, Zhang et al. 2019, Liang, Zhang et al. 2019) conducted series of studies distinguishing between simultaneous (spatial) and successive (temporal) multiple drop impacts. For simultaneous impacts they observed the formation of a central liquid sheet at the collision plane. Crucially, the splashing threshold is reduced in this regime due to the cracking or rupture of this central sheet. This rupture is initiated by surface tension forces but driven to violent splashing by gas-phase instabilities and the rapid expansion of trapped vapor bubbles on the inner crown wall.

For successive impacts, conversely, for drops impacting sequentially, the splashing threshold for the trailing droplet is higher (i.e., splashing is suppressed). This is attributed to the strong radial flow established by the leading drop, while the trailing drop impacts a fluid field that is already moving radially outward, which dissipates the impact energy and alters the kinematic discontinuity.

Thermal-Hydraulic Coupling: Liang et al. (Liang, Guo et al. 2013, Liang, Zhang et al. 2018, Liang, Zhang et al. 2019, Liang, Zhang et al. 2019) also mapped the thermal footprint of these interactions. They observed that the impact region is significantly cooler than the surrounding film due to the impingement of supercooled mass. Interestingly, the temperature of the rising crown sheet was found to be much higher than that of the central liquid sheet. Since both structures are unsaturated, this thermal contrast serves as a passive tracer, confirming that the mass constituting the crown originates primarily from the warmer pre-existing liquid film, whereas the central sheet is composed largely of the cooler impinging droplet fluid. This uneven temperature distribution, coupled with localized hot spots where vapor bubbles form, creates thermal gradients that further influence the breakup instability.

5. Environmental and Surface State Factors

5.1. Temperature Effect

Most studies of drop impacting liquid films and dry surfaces do not consider the temperature change, phase change, subcooling and film interacting with the underneath surface itself (Myers, Charpin et al. 2002, Roisman and Tropea 2002, Rioboo, Bauthier et al. 2003, Cossali, Marengo et al. 2004, Liu, Chen et al. 2017, Zhu, Tu et al. 2021). The viscosity of supercooled water increases by at least three-fold as the temperature drops from 20°C to -15°C. This physical change fundamentally alters the non-dimensional scaling that governs splashing. Specifically, while the Weber number remains relatively stable (as surface tension changes are minor), the Reynolds number decreases by a factor of three, and the Ohnesorge number increases by a factor of three.

Theoretical models suggest this shift should stabilize the droplet. For instance, in the widely used Mundo correlation, the splashing parameter K scales with $\mu^{-0.25}$, implying that increased viscosity naturally lowers the propensity to splash. Experimental data confirms increasing the liquid film temperature generally promotes the transition from spreading to splashing {Vasconcelos, 2025 #166}.

Yang et al.(Yang, Zhou et al. 2022) investigated the drop impact on a freezing film and compared their results to the standard room conditions. They found that dendritic ice, or tree shaped crystalized ice, would be pushed out of the frozen film due to the impact of the SLDs. Similarly, they reported that the differences in the crown formation, where the crown lifetime increases and then decreases due to the SLDs impacting on the freezing film but not in the room temperature conditions, which monotonically increases with the film thickness. The premature shorter crown lifetime could be attributed to the presence of dendritic ice crystals. The outcome of an SLD striking a freezing water film results in fewer secondary droplets compared to a room-temperature droplet impacting a room-temperature water film at the same thickness.

Cui and Habashi (Cui and Habashi 2023) developed a dendritic freezing model for in-flight SLD impingement, capturing phase-change dynamics at subfreezing temperatures. The model simulates dendritic ice formation and growth within impacting SLDs, influencing ice morphology and adhesion. By incorporating non-equilibrium solidification kinetics, it improves predictions of ice microstructure that determine the mechanical properties of accreted ice, aiding understanding of the

 doi:10.20944/preprints202602.2010.v1

rime-to-glaze transition and runback water formation.Jia et al. (Jia, Zhang et al. 2024) numerically and experimentally studied SLD icing on rotating spinner, achieving good agreement between both approaches. They found that increasing effective tangential impact velocity increases droplet rebound and splashing, leading to higher droplet mass loss coefficient and reduced mass collection efficiency. They also observed that the icing thickness on the surface increases with the increase of the total impact velocity.

5.2. The Role of Rivulets and Ice Feathers

While much of the literature focuses on the static roughness of the substrate itself, in practical icing scenarios, the surface roughness is dynamic and self-generating. As illustrated in the work of Zhang et al. (Zhang and Hu 2014), the initial water film does not remain smooth, but it coalesces into rivulets and isolated water beads, driven by aerodynamic shear. These features act as protruding roughness elements for subsequent droplet impacts. This self-induced roughness alters the splashing threshold. Unlike a pristine surface, a surface covered in beads and rivulets presents a complex, non-uniform topography. When subsequent droplets impinge upon these sessile beads or rivulets, the effective impact angle changes locally, often resulting in off-normal collisions that lower the energy barrier for splashing. As noted in splashing studies, high roughness tends to trigger prompt splash significantly earlier than on smooth surfaces.

Furthermore, under freezing conditions, this roughness intensifies. Yang et al. (Yang, Zhou et al. 2022) observed that dendritic ice crystals. These ice features disrupt the spreading lamella of incoming droplets, causing premature crown breakup and reducing the crown lifetime. Consequently, the growing ice surface creates a feedback loop: initial roughness (beads/rivulets) triggers early splashing, which redistributes water mass to form macroscopic roughness elements like feathers and horns, which in turn generate even more violent splashing and mass loss for future droplets.

6. Impact on Ice Protection Technologies

While the Weber and Reynolds numbers provide a baseline for predicting splashing on idealized dry surfaces, they do not account for the physicochemical interaction between the fluid and the substrate. In practical aviation scenarios, the surface condition varies significantly, from untreated aluminum to advanced ice-phobic coatings. Consequently, the splashing threshold and post-impact morphology are heavily dictated by the surface wettability and texture.

6.1. Drop Splashing on Hydrophilic Surfaces

Conventional aircraft surfaces without any treatment usually appear to be hydrophilic. When a droplet impact such hydrophilic surfaces, the droplet could experience a sequence of dynamic stages, including initial contacting, spreading, receding, splashing, and rebounding (Rioboo, Tropea et al. 2001).

Figure 16 shows the time sequences of the dynamic droplet impinging process on a hydrophilic surface at the Weber number of ~3,100 (Liu, Li et al. 2018). As the water droplet impinges on the hydrophilic surface, it is observed that the water mass would spread out in all directions to form a pancake-like structure over the hydrophilic surface with an intense splashing of the satellite water droplets at the boundary rim. As time goes by, the pancake-like structure keeps spreading until reaching its maximum contacting area. After that, the pancake-like structure starts to recede with the water mass flowing from the spreading boundary back to the impinging center. It should be noted that, during the spreading process, a thin water film with a much larger contact area (in comparison to the projected area of the water droplet) is formed over the hydrophilic surface. A large portion of the impinged water mass is kept on the hydrophilic surface during and after the impinging process. During a SLD icing event, such a hydrophilic surface would result in a rapid and tremendous ice

 doi:10.20944/preprints202602.2010.v1

accretion over the aircraft surfaces. The supercooled water mass can easily spread and adhere to the surface due to the rapid freezing process along with the impinging hydrodynamic process.

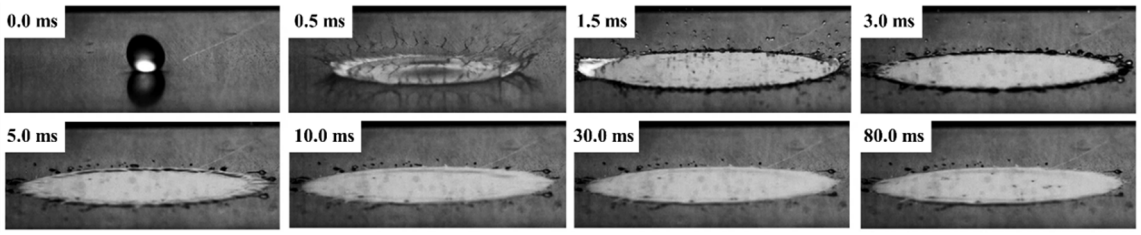

Figure 16. Time-evolutions of the dynamic impinging process of water droplets onto a hydrophilic surface at the Weber number of We ≈ 3,100 (Liu, Li et al. 2018).

6.2. Drop Splashing on Superhydrophobic Surfaces

In comparison to the hydrophilic surface, the droplet impinging process on a superhydrophobic surface appears to be very different, as shown in Figure 17 (Liu, Li et al. 2018). As the water droplet impinges onto the surface, the water mass is found to spread out rapidly to form an extremely thin water film over the superhydrophobic surface. Instead of forming a pancake-like water film, the spreading water mass is found to break into many tiny satellite droplets, which bounce off from the surface instantly. The water-repelling dynamics of this superhydrophobic surface are essentially due to the existence of the nano-/micro-scale roughness/textures on the surface. With the surface being kept at the Cassie-Baxter state, with air trapped in the surface texture beneath the droplet, the kinetic energy in the water droplet impact is not well dissipated during the spreading process, but remains in the rebounded satellite droplets. As a result, only a small portion of the impinged water mass is left on the surface after the impinging process. The remaining water mass on the surface is also found to bead up with a very large contact angle and a considerably small contact area, which is considered to be a good indicator of reduced ice adhesion strength.

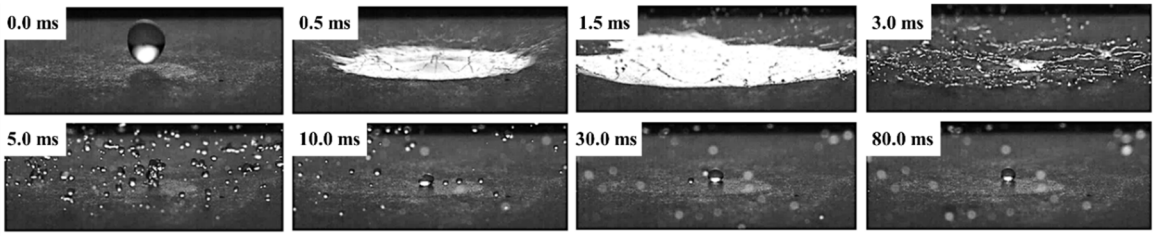

Figure 17. Time-evolutions of the dynamic impinging process of water droplets onto a superhydrophobic surface at the Weber number of We ≈ 3,100 (Liu, Li et al. 2018).

6.3. Drop Splashing on Slippery Liquid-Infused Porous Surfaces (SLIPS)

Slippery liquid-infused porous surfaces represent another class of protective surfaces capable of inhibiting droplet splashing. By impregnating a porous or textured substrate with a lubricating liquid, these surfaces form a stable, smooth liquid interface that reduces contact-line pinning and enhances viscous dissipation during impact. As a result, lubricant-infused porous surfaces can effectively suppress droplet splashing and have received growing attention in recent years. SLIPS surfaces, inspired by the Nepenthes pitcher plants, have the potential to be used as passive icephobic materials because they are able to reduce ice adhesion by 10 kPa, as measured by non-impact bulk ice (Daniel, Mankin et al. 2013, Heydarian, Jafari et al. 2021).

Figure 18 shows the snapshot images to reveal the dynamic impinging process of a water droplet on a SLIPS at the Weber number of 4,000 (Ma, Zhang et al. 2020). Upon the droplet impinging onto the SLIPS, similar spreading and splashing phenomena are observed at the early stage of the droplet

 doi:10.20944/preprints202602.2010.v1

impinging process. However, due to the hydrophobic nature of the SLIPS, the maximum spreading diameter of the water droplet on the SLIPS is found to be smaller than that over the hydrophilic surface, along with the formation of more splashing satellite droplets. During the receding process, while the contact area between the droplet and the surface becomes smaller, the inward-receding ring is found to break into more tiny water droplets. These satellite droplets are then found to coalesce and bounce off from the surface, leaving a very small amount of water mass on the SLIPS. Furthermore, unlike that of forming a large pancake-like water film on the hydrophilic surface, the remaining water mass on the SLIPS is found to break into many small droplets. Thus, the wetted area on the SLIPS becomes much smaller in comparison to that on the hydrophilic surface.

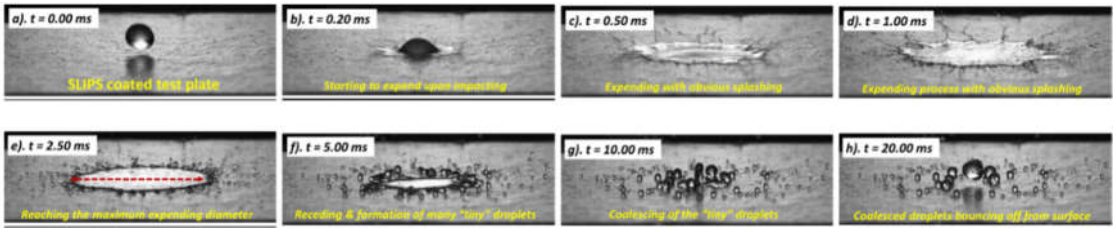

Figure 18. Time-evolutions of the dynamic impinging process of a water droplet onto a SLIPS at the Weber number of *We* ≈ 4,000 (Ma, Zhang et al. 2020).

Islam and Lian (Islam and Lian 2023)investigated moderate to high speed impacts on slippery lubricated surfaces. They investigated bare surfaces with lubricant films and porous micro-well structure that holds the lubricant. With the lubricant films without any underneath structure they found that splashing phenomena is very different at different impact speeds. For speed impacts at 5 m/s, the water drop-lubricant travels laterally, but if the speed of impact is increased by 6 folds at 30 m/s, the water drop creates a secondary impingement and recirculatory disturbance, as shown in Figure 19.

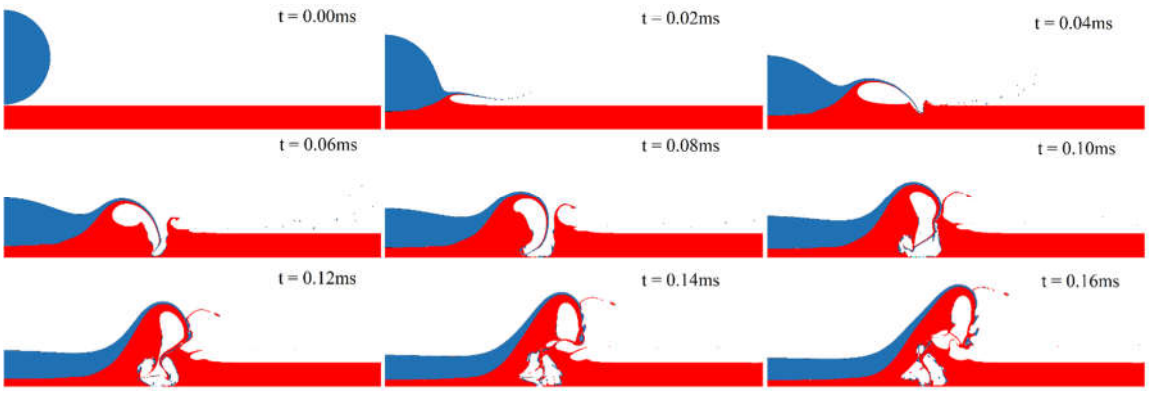

Figure 19. Drop impact on lubricant at 30 m/s, showing secondary impingement (Islam and Lian 2023).

6.4. Drop Splashing on Soft PDMS Surface

Figure 20 shows the snapshot images to reveal the dynamic impinging process of a water droplet on a soft PDMS surface at the Weber number of 4,000 (Liu, Ma et al. 2018). Upon the impingement of the water droplet on the soft PDMS surface, the soft material is found to deform instantly due to suddenly increased impact stresses over the surface. Along with the deformation of the elastic PDMS material, the impinged water mass is found to be bounced off from the surface while it still undergoes the spreading-and-receding process. The dynamically deforming PDMS surface behaves like a trampoline, which bounces off the impinged water mass. The bounced water mass then breaks into many tiny satellite droplets, as shown in Figure 20. Thus, the wetted area on this surface can be substantially reduced, thereby mitigating the SLD icing on aircraft.

 doi:10.20944/preprints202602.2010.v1

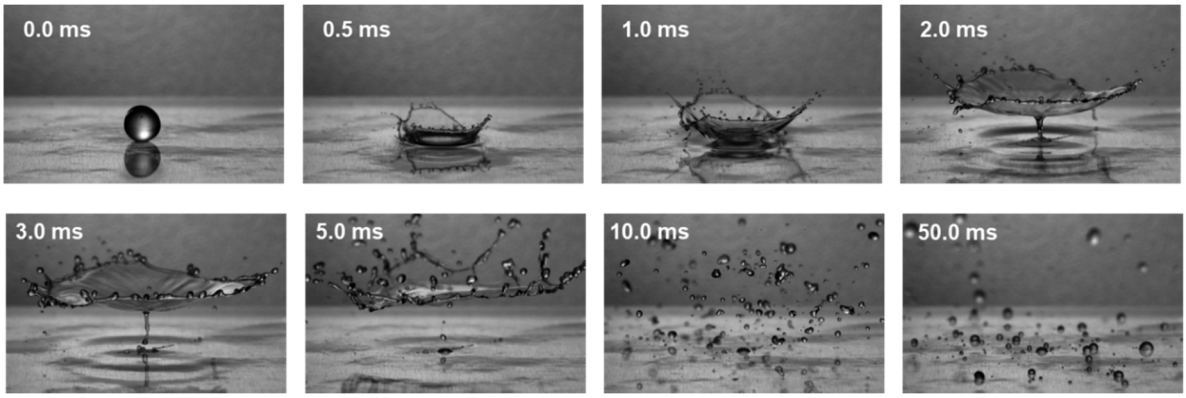

Figure 20. Time-evolutions of the dynamic impinging process of a water droplet onto a soft PDMS surface at the Weber number of *We* ≈ 4,000 (Liu, Ma et al. 2018).

While superhydrophobic surfaces, Liquid-Infused Porous Surfaces, and compliant substrates have demonstrated significant potential for mitigating SLD impacts in controlled laboratory settings (Cassie and Baxter 1945, Cao, Jones et al. 2009, Farhadi, Farzaneh et al. 2011, Ali, Qasim et al. 2018), their translation to practical aviation applications is currently impeded by severe durability and environmental stability concerns. A primary failure mode arises from thermodynamic conditions. Uunder high humidity, water condensation within the surface micro-textures can bridge the air pockets, leading to mechanical interlocking between the ice and the substrate that negates the surface's water-repellency (Meuler, McKinley et al. 2010, Nosonovsky and Hejazi 2012). Furthermore, the harsh operational envelope of flight imposes mechanical and chemical stresses rarely replicated in fundamental droplet impact studies. To maintain efficacy on a wing leading edge, these coatings must withstand high-speed rain erosion, prolonged UV radiation exposure, and intense aerodynamic shear forces without suffering texture degradation or lubricant depletion. Consequently, a significant disconnect remains between the initial aerodynamic benefits observed in the laboratory and the long-term structural integrity required for certification under realistic flight Reynolds numbers and weathering conditions.

7. Conclusions

This review has evaluated the current state of research concerning the microphysics of SLDs and their impact on aviation safety. Unlike traditional cloud-sized droplets that follow aerodynamic streamlines and freeze conformally, SLDs are governed by high inertia, leading to ballistic trajectories and impingement limits that extend well beyond the protected regions of the leading edge. SLDs alters the icing process through three primary mechanisms: extended impingement, high-speed splashing, and complex runback water dynamics. The current status of research findings can be summarized as follows:

- **Impact and Splashing Fundamentals**: Droplet impingement on dry surfaces is well-understood through regime classifications such as deposition, rebound, and splashing, with the *K* parameter serving as a primary threshold for predicting the transition to splashing. On wet surfaces, the dynamics are more complex, involving the formation of a crown-like lamella and secondary atomization that varies significantly with film thickness and ambient air conditions.
- **Modeling Constraints**: While empirical models for normal impacts at low speeds are relatively robust, a significant gap remains in characterizing high-speed, oblique impacts. Existing splashing models often fail to account for the flight-relevant conditions SLDs encounter, particularly the influence of ambient air pressure and extreme impact angles that exacerbate mass loss and secondary impingement.
- **Surface Water Dynamics**: Runback water transforms from continuous films into discrete rivulets and isolated beads under aerodynamic shear. This mass redistribution is the primary driver of non-linear, uncontrolled ice growth, yet it remains one of the most computationally

 doi:10.20944/preprints202602.2010.v1

challenging aspects to simulate due to the coupled nature of the boundary layer airflow and the multiphase water-ice interface.

- **Mitigation Strategies**: Advances in material science, including superhydrophobic surfaces and slippery liquid-infused porous surfaces, offer promising pathways for reducing droplet adhesion and promoting early shedding. However, the durability of these treatments under high-speed SLD impact and harsh environmental conditions remains a key barrier to widespread implementation.

Reference

Agbaglah, G. and R. Deegan (2014). "Growth and instability of the liquid rim in the crown splash regime." Journal of fluid mechanics **752**: 485–496.

Alghoul, S. K., C. N. Eastwick and D. B. Hann (2011). "Normal droplet impact on horizontal moving films: an investigation of impact behaviour and regimes." Experiments in Fluids **50**(5): 1305–1316.

Ali, H. M., M. A. Qasim, S. Malik and G. Murtaza (2018). "Techniques for the fabrication of super-hydrophobic surfaces and their heat transfer applications." Heat Transf. Models Methods Appl **1**: 283–315.

Allen, R. F. (1975). "The role of surface tension in splashing." Journal of Colloid and Interface Science **51**(2): 350–351.

Allen, R. F. (1975). "The role of surface tension in splashing."

Almohammadi, H. and A. Amirfazli (2019). "Droplet impact: Viscosity and wettability effects on splashing." Journal of Colloid and Interface Science **553**: 22–30.

Anderson, D. N. and J.-C. Tsao (2008). Ice shape scaling for aircraft in SLD conditions.

Ashida, T., M. Watanabe, K. Kobayashi, H. Fujii and T. Sanada (2020). "Hidden prompt splashing by corona splashing at drop impact on a smooth dry surface." Physical Review Fluids **5**(1): 011601.

Bao, M. L., Z. H. Yi, D. H. Zhao, H. Liu, Y. L. Guo, L. Y. Gong and S. Q. Shen (2025). "Dynamic characteristics of oblique droplet impact on a liquid film." Physics of Fluids **37**(2).

Bartolo, D., C. Josserand and D. Bonn (2006). "Singular jets and bubbles in drop impact." Physical review letters **96**(12): 124501.

Bernard, R., D. Baumgartner, G. Brenn, C. Planchette, B. Weigand and G. Lamanna (2021). "Miscibility and wettability: how interfacial tension influences droplet impact onto thin wall films." Journal of fluid mechanics **908**: A36.

Bhola, R. and S. Chandra (1999). "Parameters controlling solidification of molten wax droplets falling on a solid surface." Journal of materials science **34**(19): 4883–4894.

Bidwell, C. (2005). Icing calculations for a 3D, high-lift wing configuration. 43rd AIAA Aerospace Sciences Meeting and Exhibit.

Bird, J. C., S. S. Tsai and H. A. Stone (2009). "Inclined to splash: triggering and inhibiting a splash with tangential velocity." New Journal of Physics **11**(6): 063017.

Bond, T., M. Potapczuk and D. Miller (2003). Overview of SLD engineering tool development. 41st Aerospace Sciences Meeting and Exhibit.

Brackbill, J. U., D. B. Kothe and C. Zemach (1992). "A continuum method for modeling surface tension." Journal of computational physics **100**(2): 335–354.

Bragg, M. (1996). Aerodynamics of supercooled-large-droplet ice accretions and the effect on aircraft control. Proceedings of the FAA International Conference on Aircraft Inflight Icing.

Bragg, M., G. Gregorek and J. Lee (1986). "Airfoil aerodynamics in icing conditions." Journal of Aircraft **23**(1): 76–81.

Bragg, M. B., A. P. Broeren and L. A. Blumenthal (2005). "Iced-airfoil aerodynamics." Progress in Aerospace Sciences **41**(5): 323–362.

Brant Foote, G. (1973). "A numerical method for studying liquid drop behavior: Simple oscillation." Journal of Computational Physics **11**(4): 507–530.

Burzynski, D. A. and S. E. Bansmer (2019). "Role of surrounding gas in the outcome of droplet splashing." Physical Review Fluids **4**(7): 073601.

 doi:10.20944/preprints202602.2010.v1

Burzynski, D. A., I. V. Roisman and S. E. Bansmer (2020). "On the splashing of high-speed drops impacting a dry surface." Journal of Fluid Mechanics **892**: A2.

Burzynski, D. A., I. V. Roisman and S. E. Bansmer (2020). "On the splashing of high-speed drops impacting a dry surface." Journal of Fluid Mechanics **892**.

Bussmann, M., S. Chandra and J. Mostaghimi (2000). "Modeling the splash of a droplet impacting a solid surface." Physics of fluids **12**(12): 3121–3132.

Bussmann, M., J. Mostaghimi and S. Chandra (1999). "On a three-dimensional volume tracking model of droplet impact." Physics of Fluids **11**(6): 1406–1417.

Cao, L., A. K. Jones, V. K. Sikka, J. Wu and D. Gao (2009). "Anti-icing superhydrophobic coatings." Langmuir **25**(21): 12444–12448.

Cao, Y., Z. Wu and Z. Xu (2014). "Effects of rainfall on aircraft aerodynamics." Progress in Aerospace Sciences **71**: 85–127.

Cassie, A. and S. Baxter (1945). "Large contact angles of plant and animal surfaces." Nature **155**(3923): 21–22.

Castillo-Orozco, E., A. Davanlou, P. K. Choudhury and R. Kumar (2015). "Droplet impact on deep liquid pools: Rayleigh jet to formation of secondary droplets." Physical Review E **92**(5): 053022.

Cebeci, T. and F. Kafyeke (2003). "Aircraft icing." Annual review of fluid mechanics **35**(1): 11–21.

Chandra, S. and C. Avedisian (1991). "On the collision of a droplet with a solid surface." Proceedings of the Royal Society of London. Series A: Mathematical and Physical Sciences **432**(1884): 13–41.

Che, Z. and O. K. Matar (2018). "Impact of droplets on immiscible liquid films." Soft Matter **14**(9): 1540–1551.

Chen, N., H. Chen and A. Amirfazli (2017). "Drop impact onto a thin film: Miscibility effect." Physics of Fluids **29**(9).

Chen, N., H. Chen and A. Amirfazli (2017). "Drop impact onto a thin film: Miscibility effect." Physics of Fluids **29**(9): 092106.

Cheng, M. and J. Lou (2015). "A numerical study on splash of oblique drop impact on wet walls." Computers & Fluids **115**: 11–24.

Ching, B., M. W. Golay and T. J. Johnson (1984). "Droplet Impacts Upon Liquid Surfaces." Science **226**(4674): 535–537.

Cossali, G., M. Marengo and M. Santini (2004). Impact of single and multiple drop array on a liquid film. 19th Annual Meeting of ILASS, Nottingham, UK, 06-08/09/2004, ILASS Europe.

Cossali, G. E., A. Coghe and M. Marengo (1997). "The impact of a single drop on a wetted solid surface." Experiments in fluids **22**(6): 463–472.

Cossali, G. E., M. Marengo, A. Coghe and S. Zhdanov (2004). "The role of time in single drop splash on thin film." Experiments in Fluids **36**(6): 888–900.

Cui, X. D. and W. G. Habashi (2023). "A dendritic freezing model for in-flight supercooled large droplets impingement and solidification." Computers & Fluids **254**.

Daniel, D., M. N. Mankin, R. A. Belisle, T.-S. Wong and J. Aizenberg (2013). "Lubricant-infused micro/nano-structured surfaces with tunable dynamic omniphobicity at high temperatures." Applied Physics Letters **102**(23): 231603.

De Goede, T., N. Laan, K. De Bruin and D. Bonn (2017). "Effect of wetting on drop splashing of Newtonian fluids and blood." Langmuir **34**(18): 5163–5168.

Deegan, R., P. Brunet and J. Eggers (2007). "Complexities of splashing." Nonlinearity **21**(1): C1.

Driscoll, M. M. and S. R. Nagel (2011). "Ultrafast interference imaging of air in splashing dynamics." Physical review letters **107**(15): 154502.

Farhadi, S., M. Farzaneh and S. A. Kulinich (2011). "Anti-icing performance of superhydrophobic surfaces." Applied Surface Science **257**(14): 6264–6269.

Fukai, J., Y. Shiiba, T. Yamamoto, O. Miyatake, D. Poulikakos, C. M. Megaridis and Z. Zhao (1995). "Wetting effects on the spreading of a liquid droplet colliding with a flat surface: experiment and modeling." Physics of fluids **7**(2): 236–247.

Fullana, J. M. and S. Zaleski (1999). "Stability of a growing end rim in a liquid sheet of uniform thickness." Physics of Fluids **11**(5): 952–954.

 doi:10.20944/preprints202602.2010.v1

García-Geijo, P., E. Quintero, G. Riboux and J. Gordillo (2021). "Spreading and splashing of drops impacting rough substrates." Journal of Fluid Mechanics **917**.

Geppert, A., D. Chatzianagnostou, C. Meister, H. Gomaa, G. Lamanna and B. Weigand (2016). "Classification of impact morphology and splashing/deposition limit for n-hexadecane." Atomization and Sprays **26**(10).

Geppert, A., A. Terzis, G. Lamanna, M. Marengo and B. Weigand (2017). "A benchmark study for the crown-type splashing dynamics of one-and two-component droplet wall–film interactions." Experiments in Fluids **58**(12): 1–27.

Gordillo, L., T.-P. Sun and X. Cheng (2018). "Dynamics of drop impact on solid surfaces: evolution of impact force and self-similar spreading." Journal of Fluid Mechanics **840**: 190–214.

Gueyffier, D. and S. Zaleski (1998). "Formation de digitations lors de l'impact d'une goutte sur un film liquide." Comptes Rendus de l'Académie des Sciences-Series IIB-Mechanics-Physics-Astronomy **326**(12): 839–844.

Guo, Y. and Y. Lian (2017). "High-speed oblique drop impact on thin liquid films." Physics of Fluids **29**(8): 082108.

Guo, Y. and Y. Lian (2018). "Numerical investigation of oblique impact of multiple drops on thin liquid film." Journal of colloid and interface science **530**: 586–594.

Guo, Y., Y. Lian and M. Sussman (2016). "Investigation of drop impact on dry and wet surfaces with consideration of surrounding air." Physics of Fluids **28**(7): 073303.

Haller, K., D. Poulikakos, Y. Ventikos and P. Monkewitz (2003). "Shock wave formation in droplet impact on a rigid surface: lateral liquid motion and multiple wave structure in the contact line region." Journal of Fluid Mechanics **490**: 1–14.

Hansman Jr, R. J. and S. R. Turnock (1989). "Investigation of surface water behavior during glaze ice accretion." Journal of Aircraft **26**(2): 140–147.

Hao, J. (2017). "Effect of surface roughness on droplet splashing." Physics of Fluids **29**(12): 122105.

Hao, J. and S. I. Green (2017). "Splash threshold of a droplet impacting a moving substrate." Physics of Fluids **29**(1): 012103.

Hardalupas, Y., A. M. K. P. Taylor and J. H. Wilkins (1999). "Experimental investigation of sub-millimetre droplet impingement on to spherical surfaces." International Journal of Heat and Fluid Flow **20**(5): 477–485.

Heydarian, S., R. Jafari and G. Momen (2021). "Recent progress in the anti-icing performance of slippery liquid-infused surfaces." Progress in Organic Coatings **151**: 106096.

Honsek, R., W. G. Habashi and M. S. Aubé (2008). "Eulerian modeling of in-flight icing due to supercooled large droplets." Journal of aircraft **45**(4): 1290–1296.

Howland, C. J., A. Antkowiak, J. R. Castrejón-Pita, S. D. Howison, J. M. Oliver, R. W. Style and A. A. Castrejón-Pita (2016). "It's Harder to Splash on Soft Solids." Physical Review Letters **117**(18): 184502.

Islam, A. and Y. Lian (2023). "Numerical study of drop impact on slippery lubricated surfaces." Physics of Fluids **35**(3).

Jayaratne, O. and B. J. Mason (1964). "The coalescence and bouncing of water drops at an air/water interface." Proceedings of the Royal Society of London. Series A. Mathematical and Physical Sciences **280**(1383): 545–565.

Jia, W., F. Zhang and Z. Q. Zhang (2024). "Numerical and experimental investigation of the supercooled large droplets icing of rotating spinner." Applied Thermal Engineering **257**.

Josserand, C. and S. Zaleski (2003). "Droplet splashing on a thin liquid film." Physics of fluids **15**(6): 1650–1657.

Jung, S. and R. Myong (2013). Numerical modeling for eulerian droplet impingement in supercooled large droplet conditions. 51st AIAA Aerospace Sciences Meeting including the New Horizons Forum and Aerospace Exposition.

Kim, H.-Y. and J.-H. Chun (2001). "The recoiling of liquid droplets upon collision with solid surfaces." Physics of fluids **13**(3): 643–659.

Kittel, H. M., I. V. Roisman and C. Tropea (2018). "Splash of a drop impacting onto a solid substrate wetted by a thin film of another liquid." Physical Review Fluids **3**(7): 073601.

Krechetnikov, R. and G. M. Homsy (2009). "Crown-forming instability phenomena in the drop splash problem." Journal of colloid and interface science **331**(2): 555–559.

Landsberg, B. (2008). "AOPA Safety Advisor: Aircraft Icing." AOPA Air Safety Foundation, Frederick, MD: 2.

 doi:10.20944/preprints202602.2010.v1

Latka, A., A. Strandburg-Peshkin, M. M. Driscoll, C. S. Stevens and S. R. Nagel (2012). "Creation of prompt and thin-sheet splashing by varying surface roughness or increasing air pressure." Physical review letters **109**(5): 054501.

Latka, A., A. Strandburg-Peshkin, M. M. Driscoll, C. S. Stevens and S. R. Nagel (2012). "Creation of Prompt and Thin-Sheet Splashing by Varying Surface Roughness<? format?> or Increasing Air Pressure." Physical review letters **109**(5): 054501.

Leneweit, G., R. Koehler, K. G. Roesner and G. SchÄFer (2005). "Regimes of drop morphology in oblique impact on deep fluids." Journal of Fluid Mechanics **543**: 303–331.

Lesser, M. and J. Field (1983). "The impact of compressible liquids." Annual review of fluid mechanics **15**: 97–122.

Li, H., I. V. Roisman and C. Tropea (2015). "Influence of solidification on the impact of supercooled water drops onto cold surfaces." Experiments in Fluids **56**(6): 1–13.

Li, L., X. Jia, Y. Liu and M. Su (2016). "Simulation of double droplets impact on liquid film by a simplified lattice Boltzmann model." Applied Thermal Engineering **98**: 656–669.

Lian, Y. (2014). Numerical simulation of supercooled large droplets using the moment of fluid method. 52nd Aerospace Sciences Meeting.

Liang, G., Y. Guo, Y. Yang, N. Zhen and S. Shen (2013). "Spreading and splashing during a single drop impact on an inclined wetted surface." Acta Mechanica **224**(12): 2993–3004.

Liang, G., T. Zhang, H. Chen, H. Yu and S. Shen (2019). "Successive impact of multiple droplets on liquid film." European Journal of Mechanics - B/Fluids **74**: 389–398.

Liang, G., T. Zhang, Y. Chen, L. Chen and S. Shen (2019). "Two-phase heat transfer of multi-droplet impact on liquid film." International Journal of Heat and Mass Transfer **139**: 832–847.

Liang, G., T. Zhang, H. Yu, H. Chen and S. Shen (2018). "Simultaneous Impact of Multiple Droplets on Liquid Film." Journal of Industrial and Engineering Chemistry **65**: 51–61.

Liu, Y., W.-L. Chen, L. Bond and H. Hu (2017). "An experimental study on the characteristics of wind-driven surface water film flows by using a multi-transducer ultrasonic pulse-echo technique." Physics of Fluids **29**: 012102.

Liu, Y. and H. Hu (2018). "An experimental investigation on the unsteady heat transfer process over an ice accreting airfoil surface." International Journal of Heat and Mass Transfer **122**: 707–718.

Liu, Y., L. Li, H. Li and H. Hu (2018). "An experimental study of surface wettability effects on dynamic ice accretion process over an UAS propeller model." Aerospace Science and Technology **73**: 164–172.

Liu, Y., L. Ma, W. Wang, A. K. Kota and H. Hu (2018). "An experimental study on soft PDMS materials for aircraft icing mitigation." Applied Surface Science **447**: 599–609.

Liu, Y., P. Tan and L. Xu (2015). "Kelvin–Helmholtz instability in an ultrathin air film causes drop splashing on smooth surfaces." Proceedings of the National Academy of Sciences **112**(11): 3280–3284.

Ma, L., Z. Zhang, L. Gao, Y. Liu and H. Hu (2020). "An exploratory study on using Slippery-Liquid-Infused-Porous-Surface (SLIPS) for wind turbine icing mitigation." Renewable Energy **162**: 2344–2360.

Mandre, S. and M. P. Brenner (2012). "The mechanism of a splash on a dry solid surface." Journal of Fluid Mechanics **690**: 148–172.

Mani, M., S. Mandre and M. P. Brenner (2010). "Events before droplet splashing on a solid surface." Journal of Fluid Mechanics **647**: 163–185.

Mehdizadeh, N. Z., S. Chandra and J. Mostaghimi (2004). "Formation of fingers around the edges of a drop hitting a metal plate with high velocity." Journal of Fluid Mechanics **510**: 353–373.

Meuler, A. J., G. H. McKinley and R. E. Cohen (2010). "Exploiting Topographical Texture To Impart Icephobicity." ACS Nano **4**(12): 7048–7052.

Motzkus, C., F. Gensdarmes and E. Géhin (2009). "Parameter study of microdroplet formation by impact of millimetre-size droplets onto a liquid film." Journal of aerosol science **40**(8): 680–692.

Mukherjee, S. and J. Abraham (2007). "Crown behavior in drop impact on wet walls." Physics of fluids **19**(5): 052103.

Mundo, C., M. Sommerfeld and C. Tropea (1995). "Droplet-wall collisions: experimental studies of the deformation and breakup process." International journal of multiphase flow **21**(2): 151–173.

 doi:10.20944/preprints202602.2010.v1

Mundo, C., M. Sommerfeld and C. Tropea (1998). "On the modeling of liquid sprays impinging on surfaces." Atomization and sprays **8**(6).

Myers, T., J. Charpin and C. Thompson (2002). "Slowly accreting ice due to supercooled water impacting on a cold surface." Physics of Fluids **14**.

Nikolopoulos, N., A. Theodorakakos and G. Bergeles (2005). "Normal impingement of a droplet onto a wall film: a numerical investigation." International Journal of Heat and Fluid Flow **26**(1): 119–132.

Nikolopoulos, N., A. Theodorakakos and G. Bergeles (2007). "Three-dimensional numerical investigation of a droplet impinging normally onto a wall film." Journal of computational physics **225**(1): 322–341.

Nosonovsky, M. and V. Hejazi (2012). "Why Superhydrophobic Surfaces Are Not Always Icephobic." ACS Nano **6**(10): 8488–8491.

Okawa, T., T. Shiraishi and T. Mori (2008). "Effect of impingement angle on the outcome of single water drop impact onto a plane water surface." Experiments in Fluids **44**(2): 331–339.

Palacios, J., J. Hernández, P. Gómez, C. Zanzi and J. López (2013). "Experimental study of splashing patterns and the splashing/deposition threshold in drop impacts onto dry smooth solid surfaces." Experimental Thermal and Fluid Science **44**: 571–582.

Pasandideh-Fard, M., S. Aziz, S. Chandra and J. Mostaghimi (2001). "Cooling effectiveness of a water drop impinging on a hot surface." International journal of heat and fluid flow **22**(2): 201–210.

Politovich, M. K. (1989). "Aircraft icing caused by large supercooled droplets." Journal of Applied Meteorology (1988-2005): 856–868.

Poots, G., R. W. Gent, N. P. Dart and J. T. Cansdale (2000). "Aircraft icing." Philosophical Transactions of the Royal Society of London. Series A: Mathematical, Physical and Engineering Sciences **358**(1776): 2873–2911.

POTAPCZUK, M., K. AL-KHALIL and M. VELAZQUEZ (1993). Ice accretion and performance degradation calculations with LEWICE/NS. 31st Aerospace Sciences Meeting.

Quetzeri-Santiago, M., J. Castrejón-Pita and A. Castrejón-Pita (2021). "Controlling droplet splashing and bouncing by dielectrowetting." Scientific Reports **11**(1): 21410.

Quetzeri-Santiago, M. A., A. A. Castrejón-Pita and J. R. Castrejón-Pita (2019). "The effect of surface roughness on the contact line and splashing dynamics of impacting droplets." Scientific reports **9**(1): 1–10.

Raman, K., R. Jaiman, T. Lee and H. Low (2015). "On the dynamics of crown structure in simultaneous two droplets impact onto stationary and moving liquid film." Computers & Fluids **107**: 285–300.

Range, K. and F. Feuillebois (1998). "Influence of surface roughness on liquid drop impact." Journal of colloid and interface science **203**(1): 16–30.

Rao, S. J. and S. Basu (2026). "Secondary Atomization of Droplets at Extreme Conditions." Annual Review of Fluid Mechanics **58**(1): 83–110.

Rein, M. (1993). "Phenomena of liquid drop impact on solid and liquid surfaces." Fluid dynamics research **12**(2): 61–93.

Ribeiro, D. F., A. R. Silva and M. R. Panão (2020). "Insights into Single Droplet Impact Models upon Liquid Films Using Alternative Fuels for Aero-Engines." Applied Sciences **10**(19): 6698.

Riboux, G. and J. M. Gordillo (2014). "Experiments of drops impacting a smooth solid surface: a model of the critical impact speed for drop splashing." Physical review letters **113**(2): 024507.

Rieber, M. and A. Frohn (1999). "A numerical study on the mechanism of splashing." International Journal of Heat and Fluid Flow **20**(5): 455–461.

Rioboo, R., C. Bauthier, J. Conti, M. Voue and J. De Coninck (2003). "Experimental investigation of splash and crown formation during single drop impact on wetted surfaces." Experiments in fluids **35**(6): 648–652.

Rioboo, R., C. Tropea and M. Marengo (2001). "Outcomes from a drop impact on solid surfaces." Atomization and sprays **11**(2).

Roisman, I. V., K. Horvat and C. Tropea (2006). "Spray impact: Rim transverse instability initiating fingering and splash, and description of a secondary spray." Physics of Fluids **18**(10): 102104.

Roisman, I. V., A. Lembach and C. Tropea (2015). "Drop splashing induced by target roughness and porosity: The size plays no role." Advances in colloid and interface science **222**: 615–621.

Roisman, I. V., B. Prunet-Foch, C. Tropea and M. Vignes-Adler (2002). "Multiple drop impact onto a dry solid substrate." Journal of colloid and interface science **256**(2): 396–410.

 doi:10.20944/preprints202602.2010.v1

Roisman, I. V. and C. Tropea (2002). "Impact of a drop onto a wetted wall: description of crown formation and propagation." Journal of Fluid Mechanics **472**: 373–397.

Rutkowski, A., W. Wright and M. Potapczuk (2003). Numerical study of droplet splashing and re-impingement. 41st Aerospace Sciences Meeting and Exhibit.

Samenfink, W., A. Elsäßer, K. Dullenkopf and S. Wittig (1999). "Droplet interaction with shear-driven liquid films: analysis of deposition and secondary droplet characteristics." International journal of heat and fluid flow **20**(5): 462–469.

Schmehl, R., H. Rosskamp, M. Willmann and S. Wittig (1999). "CFD analysis of spray propagation and evaporation including wall film formation and spray/film interactions." International Journal of Heat and Fluid Flow **20**(5): 520–529.

Schmidt, P. and G. Knauss (1976). "Prallzerstäubung von Flüssigkeiten bei Nichtbenetzung." Chemie Ingenieur Technik **48**(7): 659–659.

Séon, T., E. Ghabache and C. Josserand (2016). Frozen Impacted Drop: from Fragmentation to Hierarchical Crack Patterns. APS Division of Fluid Dynamics Meeting Abstracts.

Shetabivash, H., F. Ommi and G. Heidarinejad (2014). "Numerical analysis of droplet impact onto liquid film." Physics of Fluids **26**(1): 012102.

Šikalo, Š., H.-D. Wilhelm, I. Roisman, S. Jakirlić and C. Tropea (2005). "Dynamic contact angle of spreading droplets: Experiments and simulations." Physics of Fluids **17**(6): 062103.

Stober, J. L., M. Santini and K. Schulte (2025). "Characterization of splashing and regime thresholds for oblique droplet impact on thin wall films." Experimental Thermal and Fluid Science **167**.

Stone, L. D., C. M. Keller, T. M. Kratzke and J. P. Strumpfer (2014). "Search for the wreckage of Air France Flight AF 447." Statistical Science **29**(1): 69–80.

Stow, C. D. and M. G. Hadfield (1981). "An experimental investigation of fluid flow resulting from the impact of a water drop with an unyielding dry surface." Proceedings of the Royal Society of London. A. Mathematical and Physical Sciences **373**(1755): 419–441.

Sussman, M., A. S. Almgren, J. B. Bell, P. Colella, L. H. Howell and M. L. Welcome (1999). "An adaptive level set approach for incompressible two-phase flows." Journal of Computational Physics **148**(1): 81–124.

Tanguy, S. and A. Berlemont (2005). "Application of a level set method for simulation of droplet collisions." International journal of multiphase flow **31**(9): 1015–1035.

Thompson, B. E. and M. R. Marrochello (1999). "Rivulet formation in surface-water flow on an airfoil in rain." AIAA journal **37**(1): 45–49.

Thoraval, M.-J., K. Takehara, T. G. Etoh, S. Popinet, P. Ray, C. Josserand, S. Zaleski and S. T. Thoroddsen (2012). "von Kármán vortex street within an impacting drop." Physical review letters **108**(26): 264506.

Thoroddsen, S. (2002). "The ejecta sheet generated by the impact of a drop." Journal of Fluid Mechanics **451**: 373–381.

Thoroddsen, S. and J. Sakakibara (1998). "Evolution of the fingering pattern of an impacting drop." Physics of fluids **10**(6): 1359–1374.

Thoroddsen, S. T. (2002). "The ejecta sheet generated by the impact of a drop." Journal of Fluid Mechanics **451**: 373–381.

Thoroddsen, S. T., K. Takehara and T. Etoh (2012). "Micro-splashing by drop impacts." Journal of Fluid Mechanics **706**: 560–570.

Thoroddsen, S. T., M.-J. Thoraval, K. Takehara and T. Etoh (2011). "Droplet splashing by a slingshot mechanism." Physical review letters **106**(3): 034501.

Trujillo, M. and C. Lee (2001). "Modeling crown formation due to the splashing of a droplet." Physics of Fluids **13**(9): 2503–2516.

Tsai, P., M. H. Hendrix, R. R. Dijkstra, L. Shui and D. Lohse (2011). "Microscopic structure influencing macroscopic splash at high Weber number." Soft Matter **7**(24): 11325–11333.

Vander Wal, R. L., G. M. Berger and S. D. Mozes (2006). "The combined influence of a rough surface and thin fluid film upon the splashing threshold and splash dynamics of a droplet impacting onto them." Experiments in fluids **40**(1): 23–32.

Vander Wal, R. L., G. M. Berger and S. D. Mozes (2006). "Droplets splashing upon films of the same fluid of various depths." Experiments in fluids **40**(1): 33–52.

Vasquez, T. (2009). "Air France Flight 447: A detailed meteorological analysis." Weather Graphics.

Wal, R. L. V., G. M. Berger and S. D. Mozes (2006). "The splash/non-splash boundary upon a dry surface and thin fluid film." Experiments in fluids **40**(1): 53–59.

Waldman, R., Y. Liu, K. Zhang and H. Hu (2015). High-speed imaging to quantify the transient ice accretion process on a NACA 0012 airfoil. 53rd AIAA Aerospace Sciences Meeting.

Walzel, P. (1980). "Zerteilgrenze beim Tropfenprall." Chemie Ingenieur Technik **52**(4): 338–339.

Wan, T. and S.-W. Wu (2004). "Aerodynamic analysis under influence of heavy rain." J Aeronaut Astronaut Aviat **41**(3): 173–180.

Weiss, D. A. and A. L. Yarin (1999). "Single drop impact onto liquid films: neck distortion, jetting, tiny bubble entrainment, and crown formation." Journal of Fluid Mechanics **385**: 229–254.

Wright, W. and M. Potapczuk (2004). Semi-empirical modelling of SLD physics. 42nd AIAA aerospace sciences meeting and exhibit.

Wright, W. B. and M. G. Potapczuk (1996). "Computational simulation of large droplet icing."

Xu, H., Y. Liu, P. He and H. Wang (1998). "The TAR model for calculation of droplet/wall impingement."

Xu, L. (2007). "Liquid drop splashing on smooth, rough, and textured surfaces." Physical Review E **75**(5): 056316.

Xu, L., L. Barcos and S. R. Nagel (2007). "Splashing of liquids: Interplay of surface roughness with surrounding gas." Physical Review E **76**(6): 066311.

Xu, L., W. W. Zhang and S. R. Nagel (2005). "Drop splashing on a dry smooth surface." Physical review letters **94**(18): 184505.

Yang, Z., B. Zhou, Z. Yang, X. Yi, Y. Du and Z. Jin (2022). "Impingement and splashing of a supercooled large droplet on a freezing water film." International Journal of Multiphase Flow **157**: 104263.

Yarin, A. L. (2006). "Drop impact dynamics: splashing, spreading, receding, bouncing." Annual review of fluid mechanics **38**(1): 159–192.

Yarin, A. L. and D. A. Weiss (1995). "Impact of drops on solid surfaces: self-similar capillary waves, and splashing as a new type of kinematic discontinuity." Journal of fluid mechanics **283**: 141–173.

Zhang, H., X. Zhang, X. Yi, F. He, F. Niu and P. Hao (2021). "Reversed role of liquid viscosity on drop splash." Physics of Fluids **33**(5): 052103.

Zhang, K. and H. Hu (2014). An Experimental Study of the Wind-Driven Water Droplet/Rivulet Flows Over an Airfoil Pertinent to Wind Turbine Icing Phenomena. ASME 2014 4th Joint US-European Fluids Engineering Division Summer Meeting collocated with the ASME 2014 12th International Conference on Nanochannels, Microchannels, and Minichannels.

Zhang, K., T. Wei and H. Hu (2015). "An experimental investigation on the surface water transport process over an airfoil by using a digital image projection technique." Experiments in Fluids **56**(9): 1–16.

Zhang, L. V., P. Brunet, J. Eggers and R. D. Deegan (2010). "Wavelength selection in the crown splash." Physics of Fluids **22**(12).

Zhao, H.-K., B. Merriman, S. Osher and L. Wang (1998). "Capturing the behavior of bubbles and drops using the variational level set approach." Journal of Computational Physics **143**(2): 495–518.

Zhbankova, S. and A. Kolpakov (1999). "Experimental study of collisions of differently sized droplets." Colloid journal of the Russian Academy of Sciences **61**(3): 390–393.

Zheng, L. and H. Zhang (2000). "An adaptive level set method for moving-boundary problems: application to droplet spreading and solidification." Numerical Heat Transfer: Part B: Fundamentals **37**(4): 437–454.

Zhu, J., C. Tu, T. Lu, Y. Luo, K. Zhang and X. Chen (2021). "Behavior of a water droplet impacting a thin water film." Experiments in Fluids **62**.